Cell Reports

Article

Fetal growth restriction impairs hippocampal neurogenesis and cognition via Tet1 in offspring

Graphical abstract

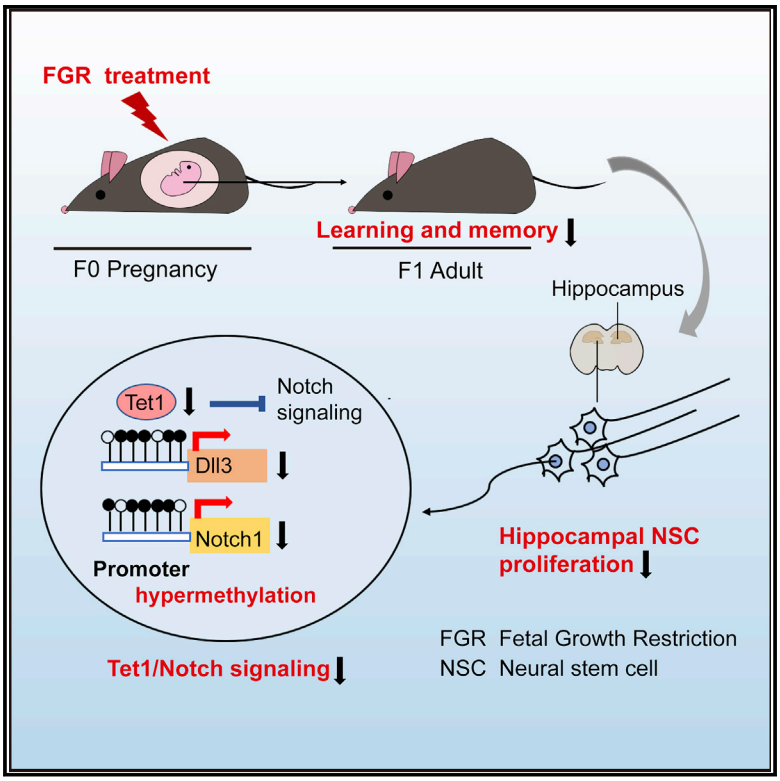

Authors

Wen Chen, Nana Liu, Shijun Shen, ..., Jiajie Xi, Cizhong Jiang, Jiuhong Kang

Correspondence

jhkang@tongji.edu.cn

In brief

Chen et al. demonstrate that fetal growth restriction (FGR) mice show decreased Tet1 expression, reduced hippocampal NSC proliferation, and impaired cognition in offspring. Increasing Tet1 activates Notch signaling, offsets the decline in neurogenesis, and enhances learning and memory abilities in FGR offspring.

Highlights

- FGR mice show decreased hippocampal NSC proliferation and impaired cognition
- FGR-induced loss of Tet1 contributes to reduced NSC proliferation
- Decreasing Tet1 results in DNA hypermethylation of Notch signaling genes
- Restoring Tet1 in the FGR hippocampus rescues neurogenesis and enhances cognition

Chen et al., 2021, Cell Reports *37*, 109912
November 2, 2021
https://doi.org/10.1016/j.celrep.2021.109912

CellPress

Cell Reports

CellPress
OPEN ACCESS

Article

Fetal growth restriction impairs hippocampal neurogenesis and cognition via Tet1 in offspring

Wen Chen,[1,3] Nana Liu,[1,3] Shijun Shen,[2] Wei Zhu,[1] Jing Qiao,[1] Shujuan Chang,[1] Jianfeng Dong,[1] Mingliang Bai,[1] Li Ma,[1] Shanshan Wang,[1] Wenwen Jia,[1] Xudong Guo,[1] Ang Li,[1] Jiajie Xi,[1] Cizhong Jiang,[2] and Jiuhong Kang[1,4,*]

[1]Clinical and Translational Research Center of Shanghai First Maternity and Infant Hospital, Shanghai Key Laboratory of Signaling and Disease Research, Frontier Science Center for Stem Cell Research, National Stem Cell Translational Resource Center, Collaborative Innovation Center for Brain Science, School of Life Sciences and Technology, Tongji University, Shanghai 200092, China

[2]Institute of Translational Research, Tongji Hospital, Shanghai Key Laboratory of Signaling and Disease Research, The School of Life Sciences and Technology, Tongji University, Shanghai 200092, China

[3]These authors contributed equally

[4]Lead contact

*Correspondence: jhkang@tongji.edu.cn

https://doi.org/10.1016/j.celrep.2021.109912

SUMMARY

Fetal growth restriction (FGR) increases the risk for impaired cognitive function later in life. However, the precise mechanisms remain elusive. Using dexamethasone-induced FGR and protein restriction-influenced FGR mouse models, we observe learning and memory deficits in adult FGR offspring. FGR induces decreased hippocampal neurogenesis from the early post-natal period to adulthood by reducing the proliferation of neural stem cells (NSCs). We further find a persistent decrease of Tet1 expression in hippocampal NSCs of FGR mice. Mechanistically, Tet1 downregulation results in hypermethylation of the Dll3 and Notch1 promoters and inhibition of Notch signaling, leading to reduced NSC proliferation. Overexpression of Tet1 activates Notch signaling, offsets the decline in neurogenesis, and enhances learning and memory abilities in FGR offspring. Our data indicate that a long-term decrease in Tet1/Notch signaling in hippocampal NSCs contributes to impaired neurogenesis following FGR and could serve as potential targets for the intervention of FGR-related cognitive disorders.

INTRODUCTION

Fetal or intrauterine growth restriction (FGR/IUGR), which affects approximately 5% of all newborns, is a critical pregnancy condition describing a fetus that fails to reach its full genetic growth potential (Mandruzzato et al., 2008; Gilchrist et al., 2018). FGR is not only the second leading cause of perinatal morbidity and mortality but also is strongly linked to neurodevelopmental disorders later in life (Gilchrist et al., 2018). Numerous large-scale follow-up studies have shown that children and adolescents born with FGR have learning difficulties and memory impairments, such as poorer spatial memory, lower academic achievements, and a lower intelligence quotient (Edmonds et al., 2010; Geva et al., 2006; Leitner et al., 2005). Unfortunately, there is currently no effective clinical treatment for FGR. Thus, identifying molecular targets that mediate the relationship between FGR and lifelong disorders will provide the basis for designing interventions to improve neurodevelopmental outcomes in FGR offspring.

In the mammalian hippocampus, which is the memory center of the brain, neural stem cells (NSCs) located in the dentate gyrus (DG) proliferate and differentiate into neurons and astrocytes, and these neurons integrate into the existing circuitry. This process known as neurogenesis occurs during early development, persists throughout life, and plays a prominent role in cognitive processes, such as learning and memory (Gonçalves et al., 2016). One hallmark of neurogenesis is its dynamic regulation by various physiological and pathological stimuli, such as exercise, aging, and stress (Ming and Song, 2011). Currently, studies involving animal models of FGR have revealed reduced neuron numbers, abnormal morphology, and altered connectivity in the hippocampus (Mallard et al., 2000; Dieni and Rees, 2003; Illa et al., 2013). However, the effect of FGR on hippocampal neurogenesis remains unclear.

Growing evidence indicates that the intrauterine environment can program adult-onset diseases by altering the epigenetic state of the offspring, resulting in permanent changes in gene expression patterns without altering the DNA sequence (Ding and Cui, 2017; Maccari et al., 2014). DNA methylation is the best-known epigenetic modification, and a number of aberrant DNA methylation patterns have been associated with prenatal FGR and associated diseases in both humans and animals (Ding and Cui, 2017; Hillman et al., 2015). Conventional studies of DNA methylation have focused on the presence of a methyl group on cytosine, termed 5-methylcytosine (5mC); once established, 5mC is propagated by DNA methyltransferases (Dnmts) and is generally associated with gene repression (Jaenisch and Bird, 2003). Recently, ten-eleven translocation (Tet) proteins

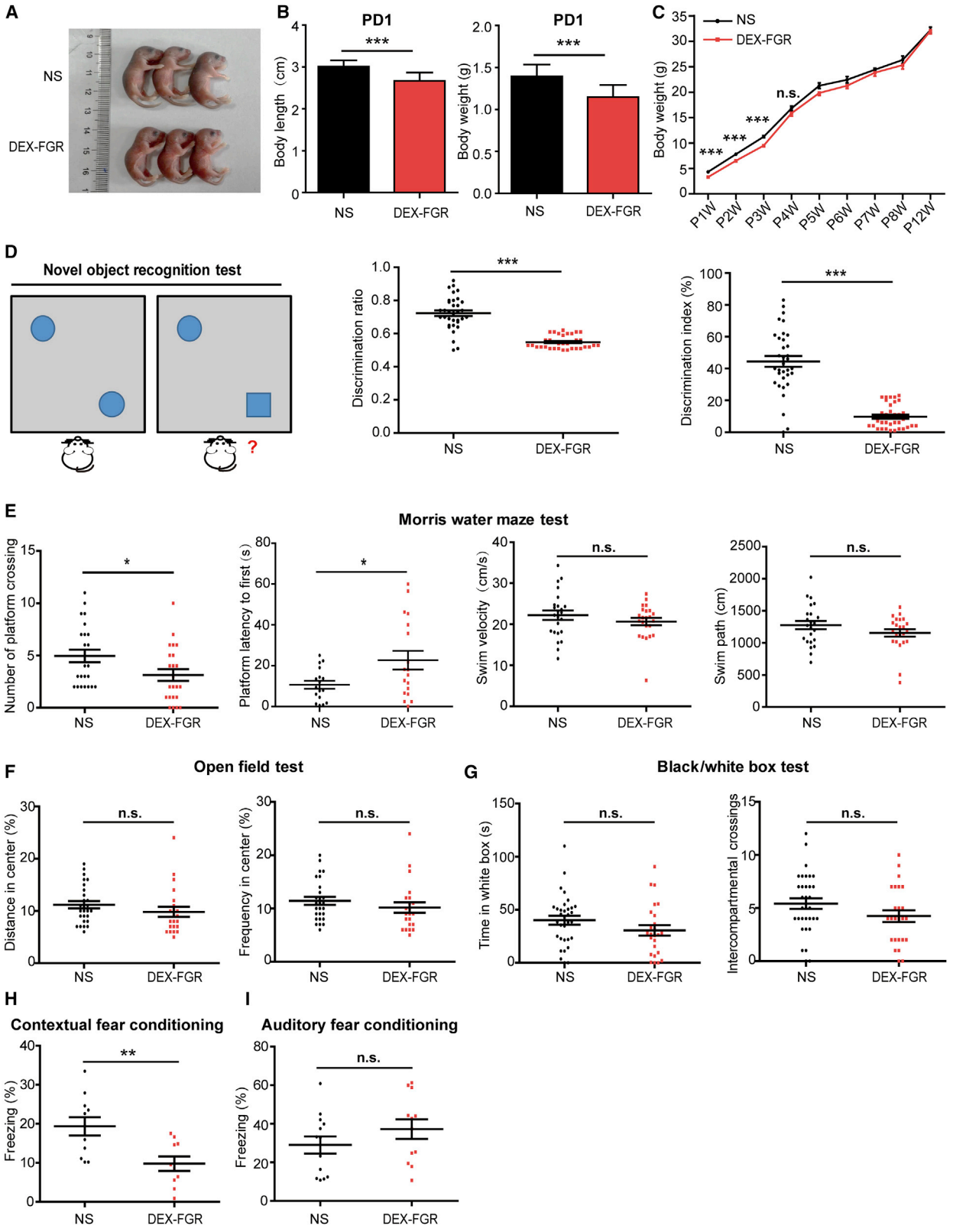

(legend on next page)

(Tet1, Tet2, Tet3) were found to initiate active DNA demethylation via oxidation of 5mC into 5-hydroxymethylcytosine (5hmC) (Wu and Zhang, 2011). Genome-wide profiling in mouse brain has shown that 5hmC enrichment at enhancers, promoters, and gene bodies is linked to specific gene expression, which indicates the critical role of Tet-mediated 5hmC modification in brain function (Szulwach et al., 2011). Indeed, multiple groups have shown that Tet1 regulates hippocampal activity-induced gene expression and mediates the consolidation and extinction of memory (Kaas et al., 2013; Rudenko et al., 2013). Tet1 deletion also leads to a reduction in adult NSC number and impairment of hippocampal neurogenesis accompanied by poor learning and memory abilities (Zhang et al., 2013), and reducing Tet2 expression in the hippocampus decreases the number of adult NSCs and impairs cognitive function (Gontier et al., 2018). However, it remains unknown whether Tet proteins are involved in FGR-associated learning and memory dysfunction.

In the investigation of the mechanisms by which FGR predisposes an individual to disease development later in life, several animal models have been developed according to the causes of FGR, in particular, exposure to glucocorticoid (GC) to mimic either maternal chronic stress or excessive administration of therapeutic GC and prenatal protein restriction (PR) to represent maternal undernutrition (Swanson and David, 2015). These two widely used models show similar neuroendocrine and clinical characteristics, for example, an adverse GC environment *in utero*, disturbance of the hypothalamic-pituitary-adrenal (HPA) axis, and decreases in brain weight, suggesting that the two usual FGR models may induce neurodevelopmental disorders in part by a common mechanism (Lesage et al., 2001; Abul et al., 2019; Liu et al., 2015). In this study, we established FGR mouse models through either prenatal overexposure to dexamethasone (DEX; a synthetic GC analog) or a prenatal PR diet and showed that FGR decreases hippocampal neurogenesis from the early post-natal period to adulthood and impairs the learning and memory abilities in adult offspring in both mouse models. Then, we discovered that Tet1/Notch signaling plays an important role in this process, providing molecular targets for the intervention of FGR-induced long-term cognitive impairment.

RESULTS

Adult FGR mice exhibit impaired hippocampal-dependent learning and memory

According to previously reported methods (Abul et al., 2019; Liu et al., 2015), we first established two FGR models in mice: DEX-induced FGR (DEX-FGR) and PR-influenced FGR (PR-FGR). As expected, the body weight and length at post-natal day (PD) 1 of both DEX-FGR and PR-FGR pups were significantly reduced (Figures 1A and 1B; Figures S1A and S1B). In the two models, FGR pups did not achieve a normal body weight during the post-natal 3-week (P3W) period, but catch-up was observed in FGR adult offspring (Figure 1C; Figure S1C). Previous work showed that maternal low PR in rats leads to increased exposure of the fetus to GCs (Lesage et al., 2001). In the PR-FGR mouse model, we tested plasma cortisol levels in both pregnant mothers and fetuses on day 18.5 of gestation, as well as pups at P3W. Both PR-FGR pregnant mothers and offspring showed higher plasma cortisol levels than controls (Figure S1D). In addition, quantitative PCR (qPCR) results showed that the expression level of placental 11β-HSD2, which rapidly inactivates physiological GCs, was lower in the PR-FGR group than in the control group (Figure S1E). Neuroimaging and histopathological studies demonstrated that FGR reduces the size of hippocampus in human infants and animal fetuses (Lodygensky et al., 2008; Mallard et al., 1999). By Nissl staining, we observed that the total volume of the hippocampus was significantly decreased in both DEX-FGR and PR-FGR mice compared with that of the respective control group at P3W. However, there was no significant difference between the two groups at post-natal 8-week (P8W) (Figures S1F and S1I).

To test whether hippocampal-dependent learning and memory function are altered in FGR offspring, we examined mouse behaviors using novel object recognition and the Morris water maze test. In the two mouse FGR models, adult FGR mice displayed decreased memory performance, as evaluated by a significantly decreased discrimination ratio and index in the novel object recognition test (Figure 1D; Figure S2A). In the Morris water maze test, the swimming velocity and path were not significantly different between the two groups; however, FGR mice displayed a significantly decreased number of platform crossings and took more time to arrive at the platform during testing, which suggests that FGR offspring have impaired learning and memory function (Figure 1E; Figure S2B). Previous studies have shown that individual differences in anxiety may influence spatial learning and memory (Herrero et al., 2006). To exclude the possible impact of anxiety, we assessed anxiety-like behaviors with the open-field and black/white box paradigms. Compared with the control mice, both DEX-FGR and PR-FGR mice showed no difference in the distance and time spent exploring the center of the open field (Figure 1F; Figure S2C). The time spent in the white compartment and the number of intercompartmental

Figure 1. DEX-FGR mice show hippocampal-dependent learning and memory defects

(A) Representative photographs of NS (normal saline) and DEX-FGR pups at PD1.

(B) Average body weight and body length of NS and DEX-FGR pups at PD1 (n = 22).

(C) Growth curves of NS and DEX-FGR mice from post-natal 1- week (P1W) to 12- week (P12W) (n = 8).

(D) Discrimination ratio and discrimination index of the novel object recognition test (NOR) in NS and DEX-FGR mice (NS, n = 34; DEX-FGR, n = 35).

(E) Platform crossings, the amounts of time required for the mice to first reach the platform area, swim velocity, and swim path during the Morris water maze test in NS and DEX-FGR mice (NS, n = 24; DEX-FGR, n = 23).

(F and G) The open-field test (F) (NS, n = 27; DEX-FGR, n = 22) and black/white box test (G) (NS, n = 33; DEX-FGR, n = 25) showed no significant behavioral differences between NS and DEX-FGR mice.

(H) The contextual fear conditioning test indicated the impaired contextual memory of DEX-FGR mice (NS, n = 11; DEX-FGR, n = 10).

(I) The auditory fear conditioning test showed no significant differences in the two groups (NS, n = 13; FGR, n = 12).

The data are shown as mean ± SEM. Two-tailed Student's t test, *p < 0.05, **p < 0.01, ***p < 0.001. n.s., not significant. See also Figures S1 and S2 and Table S1.

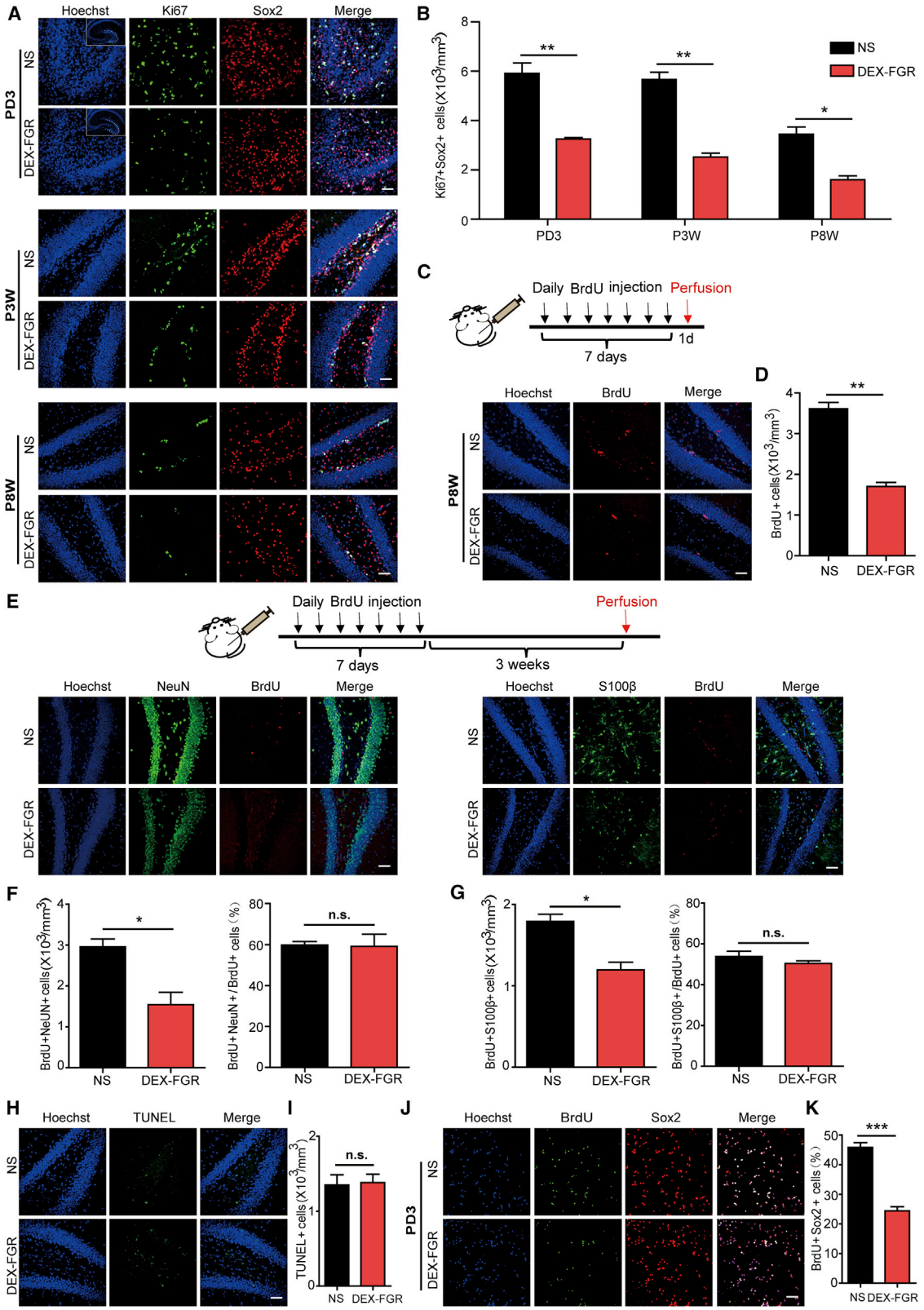

(legend on next page)

crosses were similar between the FGR and control groups (Figure 1G; Figure S2D), suggesting that the observed learning and memory impairments of FGR mice are not related to differences in basal anxiety levels. We further examined learning and memory using the fear conditioning paradigm. Contextual fear memory depends on the hippocampus, and the amygdala is critical for auditory fear memory (LeDoux, 2000). Both DEX-FGR and PR-FGR mice showed significantly less freezing than control groups in the contextual fear test (Figure 1H; Figure S2E), but there was no change in freezing in the auditory fear test (Figure 1I; Figure S2F). Taken together, these behavioral data provide evidence that adult DEX-FGR and PR-FGR mice exhibit hippocampal-dependent learning and memory deficits.

FGR mice show decreased NSC proliferation and inhibited hippocampal neurogenesis

We next asked whether FGR alters hippocampal neurogenesis in offspring. Immunohistochemical analysis showed that the number of proliferating NSCs represented by $Sox2^+Ki67^+$ cells was significantly decreased in both DEX-FGR and PR-FGR mice compared with control mice on PD3, P3W, and P8W (Figures 2A and 2B; Figures S3A and S3B). Then, 5-bromo-2′-deoxyuridine (BrdU) injection was given daily for 7 days to adult mice, which were sacrificed 1 day after the last injection. Immunostaining showed the number of $BrdU^+$ cells in the DG of both DEX-FGR and PR-FGR mice were significantly lower than those in the DG of control mice (Figures 2C and 2D; Figures S3C and S3D). Three weeks after 7-day BrdU labeling as illustrated in Figure 2E, the numbers of $BrdU^+NeuN^+$ cells and $BrdU^+S100\beta^+$ cells were significantly decreased in both DEX-FGR and PR-FGR mice. However, the percentages of $BrdU^+NeuN^+$ and $BrdU^+S100\beta^+$ in total $BrdU^+$ cells were not altered following FGR, which indicates that the neuronal and glial lineage commitment of NSCs was not affected (Figures 2F and 2G; Figures S3E–S3G). TUNEL assay showed no significant change in the number of apoptotic cells in FGR and control mice in the two models, suggesting that the decreased number of cells in the FGR hippocampus may not be caused by apoptosis (Figures 2H and 2I; Figures S3H and S3I). Additionally, the hippocampal NSCs of the two FGR models showed reduced proliferation, as indicated by the lower percentage of $BrdU^+Sox2^+$ cells compared with that in the control NSCs (Figures 2J and 2K; Figures S3J and S3K). Taken together, these results indicate that the reduced hippocampal neurogenesis in the DEX-FGR and PR-FGR mice may be caused by persistent decreased proliferation of NSCs.

FGR-induced decrease in Tet1 expression contributes to reduced proliferation of hippocampal NSCs

Then, we examined changes in the levels of the Tet proteins in the whole hippocampus from normal saline (NS) and DEX-FGR mice at the early post-natal developmental stage (PD3) and the hippocampal DGs from the two groups at P3W and P8W. Of the Dnmts and three known Tet proteins, only Tet1 was downregulated in the DEX-FGR hippocampus at all post-natal stages tested (Figures 3A and 3B; Figure S4A). In addition, there was no significant change in Tet1 expression in the cortex between two groups (Figure S4B). We also found decreased protein levels of Tet1 in the hippocampi of PR-FGR mice at the three developmental stages tested (Figure S4C). Next, we examined Tets and Dnmts protein expression in hippocampal NSCs and found that only Tet1 was downregulated in the DEX-FGR hippocampal NSCs (Figures S4D and S4E). Furthermore, we fixed and intracellularly immunostained the hippocampal cells for Tet1 and Sox2 and analyzed the results via flow cytometry. In agreement with cultured NSCs, we found that Tet1 expression levels in NSCs were lower in DEX-FGR mice than in controls, as indicated by the mean fluorescence intensity of Tet1 in Sox2-positive cells (Figures 3C and 3D). These data indicated that a persistent decrease in Tet1 expression in the hippocampal NSCs of FGR mice was paralleled by continuous decreases in hippocampal neurogenesis from the early post-natal period to adulthood.

We hypothesized that decreased Tet1 expression contributes to the FGR-induced decline in NSC proliferation. To test this hypothesis, we first established an *in vitro* cell system to mimic GC exposure in FGR mice. DEX significantly reduced hippocampal NSC proliferation (Figures 3E and 3F) and Tet1 protein expression (Figure 3G). Next, we abrogated Tet1 expression in NSCs using a lentiviral-mediated short hairpin RNA (shRNA) approach and validated its efficiency in hippocampal NSCs (Figure 3H). Tet1 knockdown significantly decreased the percentage of proliferating cells but did not further reduce the NSC proliferation rate in the presence of DEX, suggesting that Tet1 may serve as an important downstream target in hippocampal NSCs to decrease proliferation in response to DEX (Figures 3I and 3J). To further examine whether the enzymatic activity of Tet1 is responsible for these effects, we overexpressed the human Tet1 catalytic domain (OE Tet1) or a catalytically inactive Tet1

Figure 2. Impaired NSC proliferation and hippocampal neurogenesis in DEX-FGR mice

(A) Immunostaining for Ki67 and Sox2 in the hippocampal DGs of NS and DEX-FGR mice at PD3, P3W, and P8W. Dashed lines outline the calculation area in the DG at PD3. Scale bar, 50 μm.

(B) Quantification of $Ki67^+Sox2^+$ cells in the hippocampal DGs of NS and DEX-FGR mice (n = 3/stage).

(C) Immunostaining for BrdU in the hippocampal DGs of NS and DEX-FGR mice 1 day after 7-day BrdU labeling. Scale bar, 50 μm.

(D) Quantification of $BrdU^+$ cells in NS and DEX-FGR mice (n = 3).

(E) Immunofluorescence analysis of differentiated cells in the hippocampal DGs of NS and DEX-FGR mice 3 weeks after 7-day BrdU labeling. Scale bar, 50 μm.

(F) Quantitation of mature neurons ($BrdU^+NeuN^+$) and percentage of $BrdU^+NeuN^+$ cells among the $BrdU^+$ cells labeled (n = 6).

(G) Quantitation of astrocytes ($BrdU^+S100\beta^+$) and percentage of $BrdU^+S100\beta^+$ cells among the $BrdU^+$ cells labeled (n = 3).

(H) TUNEL assay of the hippocampal DGs of NS and DEX-FGR mice at P8W. Scale bar, 50 μm.

(I) Quantification of TUNEL-positive apoptotic cells in the two groups (n = 3).

(J and K) Immunostaining (J) and quantification of the percentage of $BrdU^+Sox2^+$ cells (K) in hippocampal NSCs derived from NS and DEX-FGR mice at PD3 (n = 3). Scale bar, 100 μm.

The data are shown as mean ± SEM. Two-tailed Student's t test, *$p < 0.05$, **$p < 0.01$, ***$p < 0.001$. See also Figure S3 and Table S1.

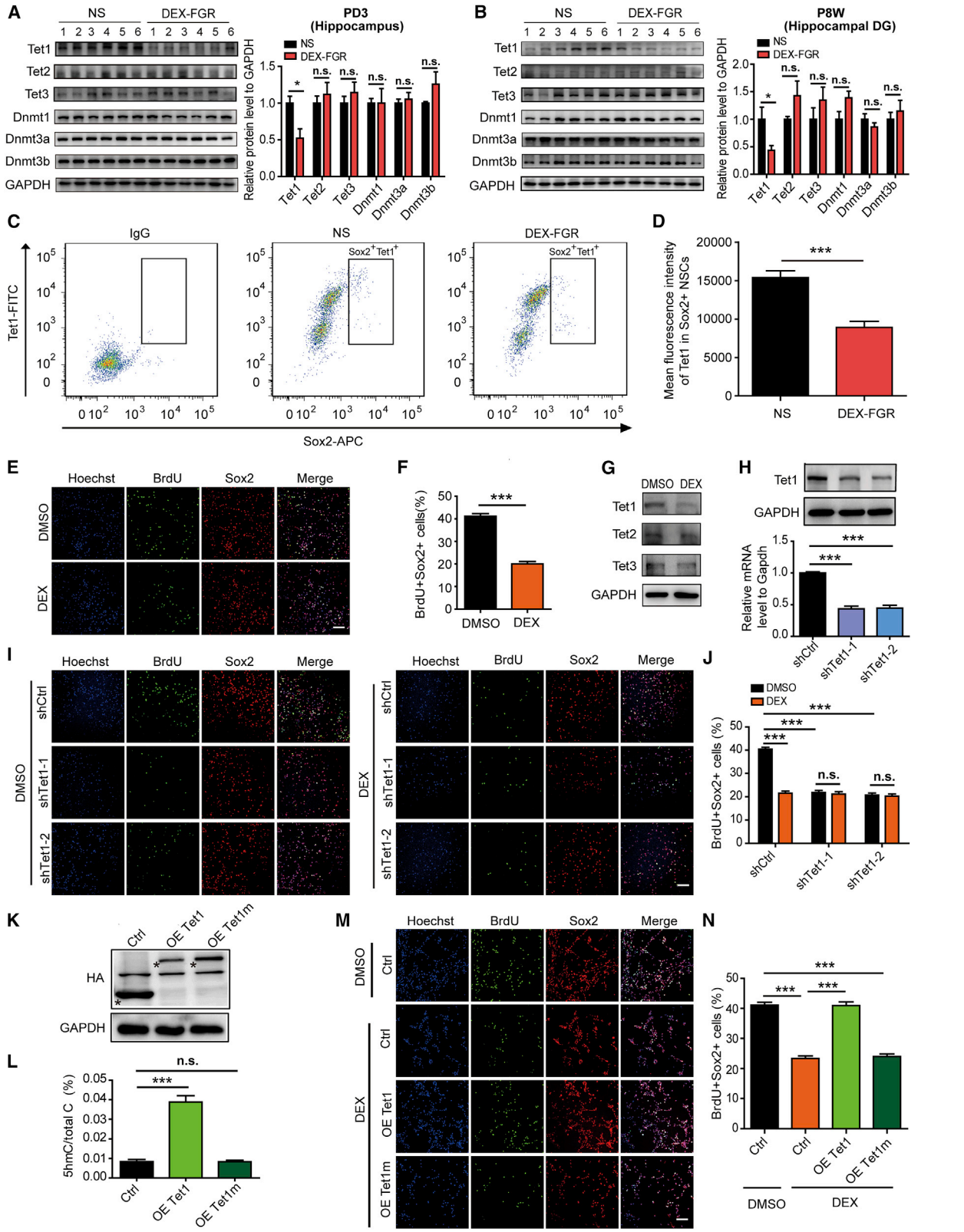

(legend on next page)

mutant (OE Tet1m) in NSCs (Figure 3K). Upon analysis of 5hmC levels, Tet1 overexpression was observed to increase the global enrichment of 5hmC, but no change was observed in NSCs overexpressing the Tet1 mutant compared with the levels in the control NSCs (Figure 3L). We found that Tet1 overexpression rescued the DEX-induced inhibition of hippocampal NSC proliferation compared with that of the control groups. In contrast, the Tet1 mutant did not have a similar effect, further highlighting the predominant role of Tet1-mediated DNA demethylation in the DEX-induced decrease in the proliferation of hippocampal NSCs (Figures 3M and 3N).

RNA sequencing (RNA-seq) reveals consistent downregulation of Notch signaling genes in the FGR hippocampus

We next used RNA-seq to capture transcriptome-wide alterations in the hippocampi of NS and DEX-FGR mice at PD3 and P8W. FGR resulted in 36 upregulated and 188 downregulated genes in the early post-natal period (PD3) and 54 upregulated and 198 downregulated genes in adults (P8W) compared with the respective genes in the NS control mice ($p < 0.05$) (Figure 4A). Interestingly, in contrast with the differentially upregulated genes in the two developmental stages, the downregulated genes were largely enriched in Gene Ontology (GO) terms that were more similar, such as "cell adhesion," "blood vessel development," and "cell proliferation" (Figure 4B). To identify genes with consistent alterations in the same direction, we reanalyzed RNA-seq data of the hippocampi from FGR mice at PD3 and P8W by gene set enrichment analysis (GSEA). GSEA results indicated that these co-downregulated gene sets were concentrated in certain meaningful categories that have pivotal roles in recognition, such as cell adhesion, blood vessel morphogenesis, and Notch signaling (Figure 4C). Notch signaling has been demonstrated to regulate NSC proliferation and is involved in learning and memory behaviors (Costa et al., 2003; Gonçalves et al., 2016). GSEA results revealed a significantly negative enrichment of Notch signaling in the hippocampus of DEX-FGR mice at both PD3 and P8W (Figure 4D).

In line with the results obtained by RNA-seq, qPCR results showed a reduction in the mRNA levels of three key Notch signaling genes, including the ligand Dll3 (Delta-like 3), receptor Notch1, and essential downstream target Hes5 (Hairy and enhancer of split-5) in the hippocampi of DEX-FGR mice at both PD3 and P8W (Figures 4E and 4G). Likewise, western blotting (WB) results showed that the protein levels of Dll3, Notch1 intracellular domain (N1ICD), and Hes5 were lower in the hippocampi of DEX-FGR mice than in the NS control offspring at both PD3 and P8W (Figures 4F and 4H). We also found decreased mRNA and protein levels of the Notch signaling genes in the hippocampi of PR-FGR mice at both PD3 and P8W (Figures S5A–S5D). In addition, hippocampal NSCs of DEX-FGR mice at PD3 and P8W showed reduced expression of Notch signaling genes (Figures S5E–S5H). Previous studies have reported that Notch1 and Hes5 positively regulate NSC proliferation (Ehm et al., 2010; Ohtsuka et al., 2001), but how Dll3 affects hippocampal NSC proliferation remains unknown. Thus, we constructed two lentiviral vectors expressing shRNAs that specifically targeted Dll3. The knockdown efficiency of the individual sequences in hippocampal NSCs was confirmed using qPCR and WB. The mRNA and protein levels of Notch1 and Hes5 and the proliferation rate of NSCs were downregulated after Dll3 knockdown, indicating that Dll3 also positively regulates NSC proliferation (Figures 4I–4K). In DEX-treated hippocampal NSCs, the decrease in NSC proliferation was accompanied by a reduction in Dll3, Notch1, and Hes5 mRNA and protein levels (Figures 4L and 4M). Moreover, we infected NSCs with the N1ICD using a lentivirus approach. The overexpression of N1ICD and its downstream gene Hes5 was confirmed by WB (Figure 4N). Notch pathway activation by N1ICD overexpression reversed the decreased cell proliferation in DEX-treated hippocampal NSCs, indicating that Notch signaling plays a major role in DEX-regulated NSC proliferation (Figures 4O and 4P). These data suggest that a constant reduction in Notch signaling may contribute to the inhibition of hippocampal NSC proliferation in FGR mice.

Reducing Tet1 is responsible for DNA hypermethylation of Notch signaling genes

Because our data showed that FGR induces long-term expression changes in Notch signaling genes in the hippocampus, we next examined whether epigenetic regulation, such as sustained reductions in Tet1 expression, is involved in the regulation of

Figure 3. Decreased Tet1 expression in the hippocampi of DEX-FGR mice is responsible for the reduced proliferation of hippocampal NSCs

(A) WB analysis showed Tet1, Tet2, Tet3, Dnmt1, Dnmt3a, and Dnmt3b expression in the hippocampi at PD3 from NS and DEX-FGR mice (n = 6).

(B) WB analysis showed Tet1, Tet2, Tet3, Dnmt1, Dnmt3a, and Dnmt3b expression in the hippocampal DGs at P8W from NS and DEX-FGR mice (n = 6).

(C) Representative fluorescence-activated cell sorting (FACS) plots of $Sox2^+Tet1^+$ cells isolated from the hippocampi of NS and DEX-FGR mice at P8W.

(D) Quantification of the mean fluorescence intensity of Tet1 in $Sox2^+$ cells from DEX-FGR mice compared with the NS group (n = 6).

(E and F) Immunostaining (E) and quantification of the percentage of $BrdU^+Sox2^+$ cells (F) in DMSO- or DEX-treated hippocampal NSCs for 48 h. Scale bar, 100 μm.

(G) WB analysis showed Tet1, Tet2, and Tet3 expression in DMSO- or DEX-treated hippocampal NSCs for 48 h.

(H) qPCR and WB analysis of Tet1 expression levels in hippocampal NSCs following Tet1 knockdown.

(I and J) Immunostaining (I) and quantification of the percentage of $BrdU^+Sox2^+$ cells (J) in Tet1 knockdown and control NSCs treated with DMSO or DEX for 48 h. Scale bar, 100 μm.

(K) WB analysis of HA in NSCs overexpressing HA-Luc (Ctrl), HA-Tet1 (OE Tet1), or HA-Tet1 mutant (OE Tet1m). The asterisk indicates specific bands.

(L) Total 5hmC level analysis of Ctrl, OE Tet1, or OE Tet1m NSCs.

(M and N) Immunostaining (M) and quantification of the percentage of $BrdU^+Sox2^+$ cells (N) in NSCs of the DMSO+Ctrl, DEX+Ctrl, DEX+OE Tet1, and DEX+ OE Tet1m groups. Scale bar, 100 μm.

The data are shown as mean ± SEM. Two-tailed Student's t test in (A), (B), (D), (F), (H) and (J); one-way ANOVA with Bonferroni multiple comparison in (L) and (N); $^*p < 0.05$, $^{***}p < 0.001$. See also Figure S4, Tables S1 and S4, and Data S1.

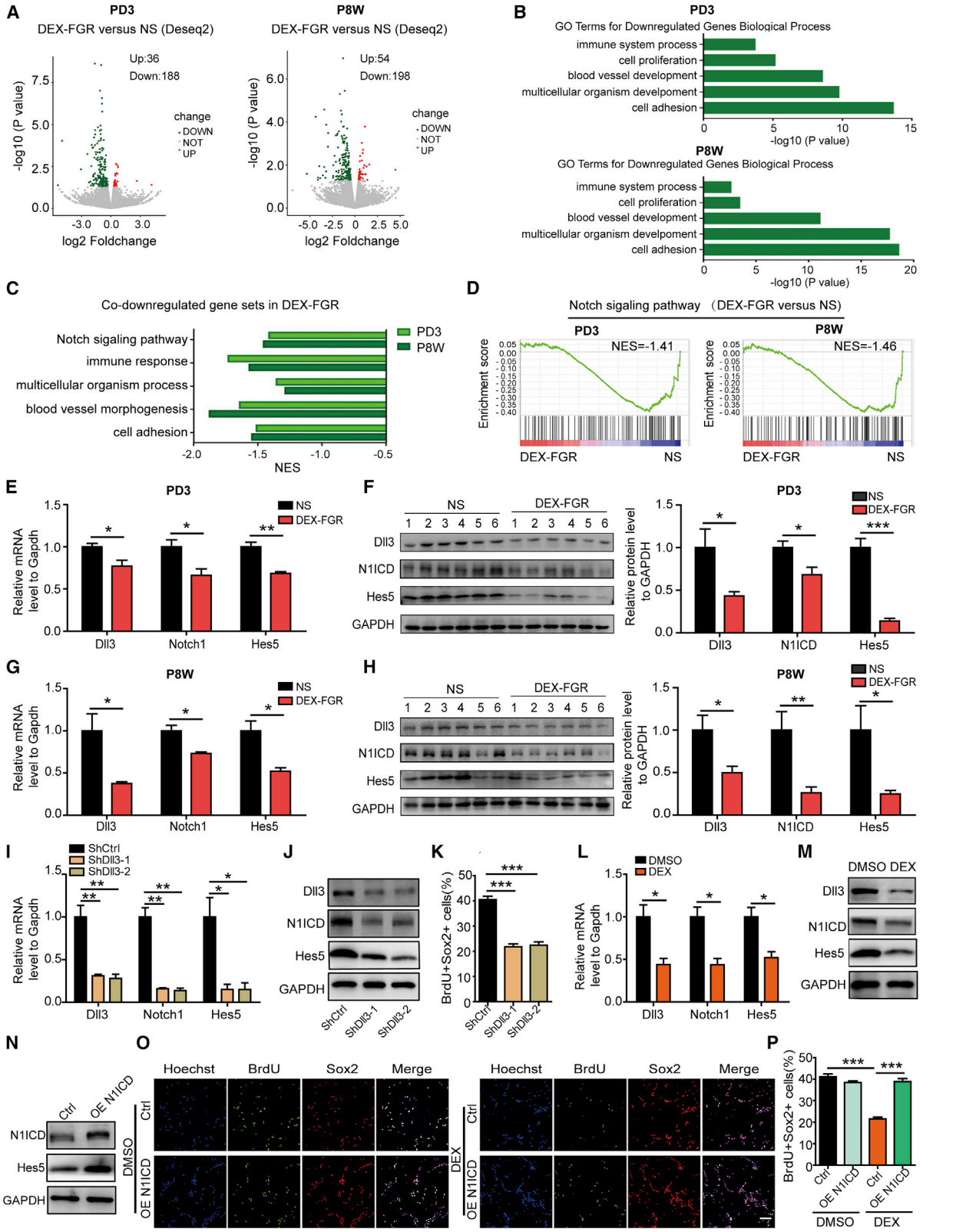

(legend on next page)

Notch signaling genes in the hippocampus of FGR mice. We compared our RNA-seq data with public RNA-seq data of the hippocampus of Tet1 knockout (KO) mice (Rudenko et al., 2013) by GSEA. There were more overlapping downregulated gene sets than upregulated gene sets between the two datasets. GSEA results also revealed negative enrichments of Notch signaling, blood vessel morphogenesis, and cell adhesion in the hippocampus of Tet1 KO mice, which is similar to the pattern of the FGR hippocampus (Figures S6A–S6C). In addition, we analyzed publicly available 5hmC profiles of the mouse hippocampus (Szulwach et al., 2011) and genes with altered expression in the hippocampus of DEX-FGR mice. The profiles shown in Figure 5A indicate that the downregulated genes were more enriched with 5hmC than the upregulated genes, implying that the regulation of downregulated genes may be partly a result of 5hmC modification (Figure 5A). Recent studies have suggested that the loss of Tet protein-associated 5hmC is concomitant with aberrant promoter hypermethylation at repressed genes (Guo et al., 2011; Wu and Zhang, 2011; Zhang et al., 2013). We hypothesized that decreased Tet1 may contribute to alterations in the expression of downregulated 5hmC-containing genes, such as Notch signaling genes, in the hippocampus of DEX-FGR mice. To test this hypothesis, we examined whether Tet1-mediated 5mC oxidation leads to DNA demethylation of endogenous Notch signaling genes. Our hydroxymethylated DNA immunoprecipitation (hMeDIP)-qPCR assay discovered a significant decrease in 5hmC content at the promoter regions of Dll3 and Notch1 in the hippocampi of DEX-FGR mice at both PD3 and P8W (Figures 5B and 5C). Chromatin immunoprecipitation (ChIP)-qPCR assays also revealed that decreased Tet1 binding at the Dll3 and Notch1 promoters coincided with Tet1 downregulation in the hippocampi of DEX-FGR mice at PD3 and P8W (Figures 5D and 5E). Using bisulfite sequencing for quantitative analysis of DNA methylation, we found significantly increased CpG methylation levels at the promoters of Dll3 and Notch1 in the hippocampi of DEX-FGR mice at PD3 and P8W compared with the levels in control offspring, which showed hypomethylation at these loci (Figures 5F and 5G). In conclusion, decreased Tet1 in the hippocampus induced DNA hypermethylation of Notch signaling genes in DEX-FGR mice. Some components of Wnt and phosphatidylinositol 3-kinase (PI3K)/AKT/mammalian target of rapamycin (mTOR) pathways have been reported as Tet1 hypomethylated targets involved in cellular proliferation (Fan et al., 2018; Good et al., 2018; Neri et al., 2015). However, qPCR analysis showed no change in the mRNA expression of these pathway genes in the hippocampi of DEX-FGR mice compared with the control group at PD3 or P8W (Figures S7A–S7D).

In addition, we evaluated the direct regulation of Tet1 on Notch signaling in hippocampal NSCs. Using hippocampal NSCs lentivirally transduced with shCtrl, shTet1-1, and shTet1-2, we found that Tet1 knockdown resulted in a significant downregulation of the three Notch signaling genes (Dll3, Notch1, and Hes5) at both the mRNA and the protein levels (Figures 5H and 5I). As expected, Tet1 knockdown NSCs showed decreased Tet1 enrichment and 5hmC levels and increased CpG methylation levels at the Dll3 and Notch1 promoters (Figures 5J–5L). Overexpression of N1ICD completely rescued the effect of Tet1 depletion on cell proliferation, as indicated by the increased percentage of proliferating $BrdU^+Sox2^+$ cells (Figure 5M). These data indicated that Notch signaling genes are directly regulated by the Tet1-dependent DNA demethylation mechanism in hippocampal NSCs. Furthermore, we asked whether Tet1 is involved in DEX-mediated inhibition of Notch signaling. We found that DEX treatment increased the levels of CpG methylation at the Dll3 and Notch1 loci, which is similar to the effects of Tet1 depletion (Figure 5N). Importantly, pharmacological blockade of Notch signaling by DAPT abrogated Tet1 overexpression-induced rescue of proliferation in DEX-treated NSCs, indicating that the DEX-induced decrease in Tet1 is responsible for the inhibited Notch signaling and reduced NSC proliferation (Figures 5O and 5P). Thus, our *in vitro* and *in vivo* results demonstrate that reducing Tet1 lowers the levels of 5hmC at Notch signaling genes and increases the levels of 5mC and 5mC-dependent transcriptional silencing.

Increasing Tet1 restores Notch signaling and ameliorates the decline in neurogenesis and memory in FGR mice

To investigate whether restoring Tet1 in the hippocampal DG could counteract FGR-related neurogenesis and cognitive decline, we utilized an *in vivo* retrovirus-mediated overexpression approach, which infected only proliferating cells (Song et al., 2013). We delivered retrovirus expressing a hemagglutinin (HA)-tagged human Tet1 catalytic domain (OE Tet1) specifically

Figure 4. DEX-FGR inhibits Notch signaling genes in the hippocampus

(A) Volcano plot of differential expression genes (DEGs) from the hippocampi of DEX-FGR mice at PD3 and the hippocampal DGs of DEX-FGR mice at P8W. Green and red dots indicate statistical DEGs.

(B) GO analysis of downregulated genes in the hippocampi of DEX-FGR mice at PD3 and the hippocampal DGs of DEX-FGR mice at P8W.

(C) GSEA results of co-downregulated gene sets hippocampi of DEX-FGR mice at PD3 and the hippocampal DGs of DEX-FGR mice at P8W.

(D) GSEA results of a significantly negative enrichment of Notch signaling in the hippocampi of DEX-FGR mice at both PD3 ($p = 0.03$) and P8W ($p = 0.01$).

(E and F) qPCR (E, $n = 3$) and WB (F, $n = 6$) analysis showed Dll3, Notch1, and Hes5 expression in the hippocampi of NS and DEX-FGR mice at PD3.

(G and H) qPCR (G, $n = 3$) and WB (H, $n = 6$) analysis showed Dll3, Notch1, and Hes5 expression in the hippocampal DGs of NS and DEX-FGR mice at P8W.

(I and J) qPCR (I) and WB (J) analysis showed Dll3, Notch1, and Hes5 expression in Dll3 knockdown and control NSCs.

(K) The percentage of $BrdU^+Sox2^+$ cells in Dll3 knockdown and control NSCs.

(L and M) qPCR (L) and WB (M) analysis of Dll3, Notch1, and Hes5 expression levels in NSCs treated with DMSO or DEX for 48 h.

(N) WB analysis of N1ICD and Hes5 expression in NSCs overexpressing HA-Luc (Ctrl) or HA-N1ICD (OE N1ICD).

(O and P) Immunostaining (O) and quantification of the percentage of $BrdU^+Sox2^+$ cells (P) in Ctrl or OE N1ICD NSCs treated with DMSO or DEX for 48 h. Scale bar, 100 μm.

The data are shown as mean ± SEM. Two-tailed Student's t test in (E)–(I), (K), and (L); one-way ANOVA with Bonferroni multiple-comparison in (P); $^*p < 0.05$, $^{**}p < 0.01$, $^{***}p < 0.001$. NES, normalized enrichment score. See also Figure S5, Tables S1 and S4, and Data S1.

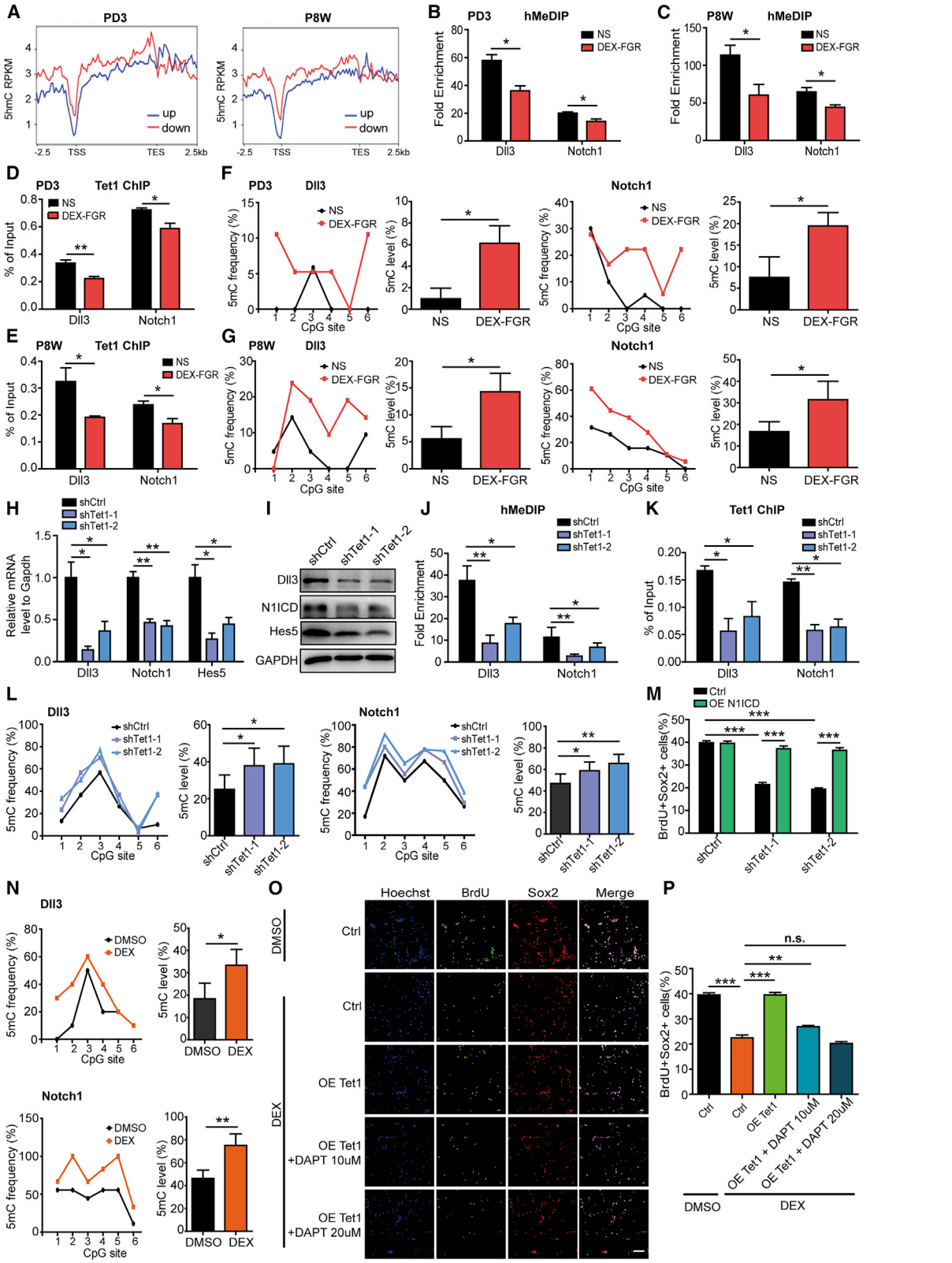

(legend on next page)

to the hippocampal DG of DEX-FGR mice via bilateral stereotactic injections. Retrovirus containing an HA-tagged luciferase gene (Ctrl) was injected into NS control or DEX-FGR mice (Figures 6A and 6B). Examination of hippocampal DGs harvested from NS and DEX-FGR mice injected with lentivirus-Ctrl revealed that the mRNA levels of Dll3, Notch1, and Hes5 were reduced in DEX-FGR mice. As expected, overexpression of Tet1 in DEX-FGR mice restored the mRNA levels of three Notch signaling genes to levels comparable with those in NS offspring (Figure 6C). Increasing Tet1 in the hippocampal DG of DEX-FGR mice also rescued the 5hmC binding and CpG methylation levels at the promoters of Dll3 and Notch1 in a statistically significant manner (Figures 6D and 6E). Then, we observed that increasing Tet1 in the hippocampi of DEX-FGR mice restored the proliferation of NSCs based on the numbers of $Ki67^{+}Sox2^{+}$ cells and $BrdU^{+}$ cells (Figures 6F–6I). Next, we examined whether Tet1 overexpression in the hippocampus was able to rescue the impaired learning and memory abilities of DEX-FGR mice. Compared with lentivirus-Ctrl-treated NS offspring, lentivirus-Ctrl-treated DEX-FGR mice exhibited a significantly lower discrimination index and ratio in the novel objective test, a decreased number of platform crossings and more time required to first reach the platform area in the Morris water maze experiment, and less freezing in the contextual fear test. However, increasing Tet1 levels rescued these learning and memory deficits in DEX-FGR mice (Figures 6J–6L). Therefore, restoring Tet1 in the adult hippocampal neurogenic niche could activate Notch signaling and counteract FGR-related neurogenesis and memory decline.

DISCUSSION

Although emerging studies have shown anatomical changes and gene expression alterations in the hippocampi of FGR offspring (Dieni and Rees, 2003; Ding and Cui, 2017; Hillman et al., 2015; Illa et al., 2013; Lodygensky et al., 2008; Mallard et al., 1999, 2000), the cellular and molecular targets responsible for hippocampal neurogenesis in FGR offspring have not been elucidated. Our data provide evidence that FGR leads to inhibited NSC proliferation, impaired learning and memory ability, and decreased expression of Tet1 and Notch signaling genes in both DEX-FGR and PR-FGR mouse offspring (Table S1), revealing previously unknown cellular and molecular mechanisms of FGR-induced long-term neurodevelopmental disorders.

Previous studies showed reductions in the total number of neurons within the hippocampus of FGR offspring (Mallard et al., 2000). The selective loss of hippocampal neurons may be caused by neuronal death or/and decreased neurogenesishttps://www.sciencedirect.com/topics/neuroscience/neurogenesis. Our TUNEL results indicated that FGR does not induce an increase in hippocampal neural cell death. Consistent with our data, immunostaining for bcl2, bax, and caspase-3 revealed no increased neuronal cell death in the hippocampi of DEX-treated rat models (Tan et al., 2002). Moreover, we observed a lasting decrease in the proliferation of NSCs in FGR offspring from the early post-natal period to adulthood, leading to a reduction in the number of newly formed neurons and astrocytes. These results are in line with data from GC-mediated inhibition of stem cell proliferation, including human embryonic, rat embryonic, and adult NSCs (Bose et al., 2010; Kim et al., 2004; Moors et al., 2012). Previous reports regarding NSC differentiation via GC treatment are controversial. Some studies support the notion that GC interferes with neuronal differentiation of NSCs (Moors et al., 2012), while other studies showed that elevated GC levels slow down the proliferation of NSCs but have no effects on their differentiation (Bose et al., 2010; Kim et al., 2004). In the present study, our data found that FGR offspring exhibit reduced hippocampal NSC proliferation and neurogenesis, but no difference in the cell lineage commitment of NSCs, which indicates that the significant decrease in the number of neurons newly generated from NSCs in FGR offspring may be caused by the decreased number of NSCs. Notably, the lack of Tet1, the altered epigenetic target associated with FGR described in this study, also decreases the self-renewal capability of adult hippocampal NSCs but does not impact their differentiation potential (Zhang et al., 2013).

Previous studies described lasting DNA methylation changes in humans and animals born with FGR (Ding and Cui, 2017; Hillman et al., 2015). Coincidently, our data showed that a significant decrease in Tet1 persists in the hippocampi of FGR offspring from the early post-natal period to adulthood, suggesting that the strong and sustained global expression changes in

Figure 5. Reducing Tet1 induces DNA hypermethylation of Notch signaling genes

(A) The 5hmC modification status of upregulated and downregulated genes in DEX-FGR mice at PD3 and P8W. 2.5 kb upstream of transcription start sites (TSSs) and downstream of transcription end sites (TESs) were included.

(B and C) hMeDIP-qPCR analysis of 5hmC level changes at the promoters of Dll3 and Notch1 in the hippocampi at PD3 (B) and the hippocampal DGs at P8W (C) from NS and DEX-FGR mice (n = 3).

(D and E) ChIP-qPCR analysis of the enrichment of Tet1 at the promoter of Dll3 and Notch1 in the hippocampi at PD3 (D) and the hippocampal DGs at P8W (E) from NS and DEX-FGR mice (PD3, n = 3, 4 mice per sample pool; P8W, n = 3, 2 mice per sample pool).

(F and G) Bisulfite sequencing analysis of CpG methylation status at the Dll3 and Notch1 promoters in the hippocampi at PD3 (F) and the hippocampal DGs at P8W (G) from NS and DEX-FGR mice (n = 3).

(H and I) qPCR (H) and WB (I) analysis of Dll3, Notch1, and Hes5 expression levels in Tet1 knockdown and control NSCs.

(J–L) hMeDIP-qPCR analysis of 5hmC level (J), ChIP-qPCR analysis of Tet1 binding (K), and bisulfite sequencing analysis of CpG methylation status (L) at Dll3 and Notch1 promoters in Tet1 knockdown and control NSCs.

(M) Quantification of the percentage of $BrdU^{+}Sox2^{+}$ cells in Tet1 knockdown or control NSCs overexpressing HA-N1ICD (OE N1ICD) or HA-Luc (Ctrl).

(N) Bisulfite sequencing analysis of Dll3 and Notch1 promoters in NSCs treated with DMSO or DEX for 48 h.

(O and P) Immunostaining (O) and quantification of the percentage of $BrdU^{+}Sox2^{+}$ cells (P) in NSCs of the DMSO+Ctrl, DEX+Ctrl, DEX+OE Tet1, DEX+OE Tet1+10 μM DAPT, and DEX+OE Tet1+20 μM DAPT groups. Scale bar, 100 μm.

The data are shown as mean ± SEM. Two-tailed Student's t test in (B)–(H) and (J)–(N); one-way ANOVA with Bonferroni multiple comparison in (P). $^{*}p < 0.05$, $^{**}p < 0.01$, $^{***}p < 0.001$. See also Figures S6 and S7.

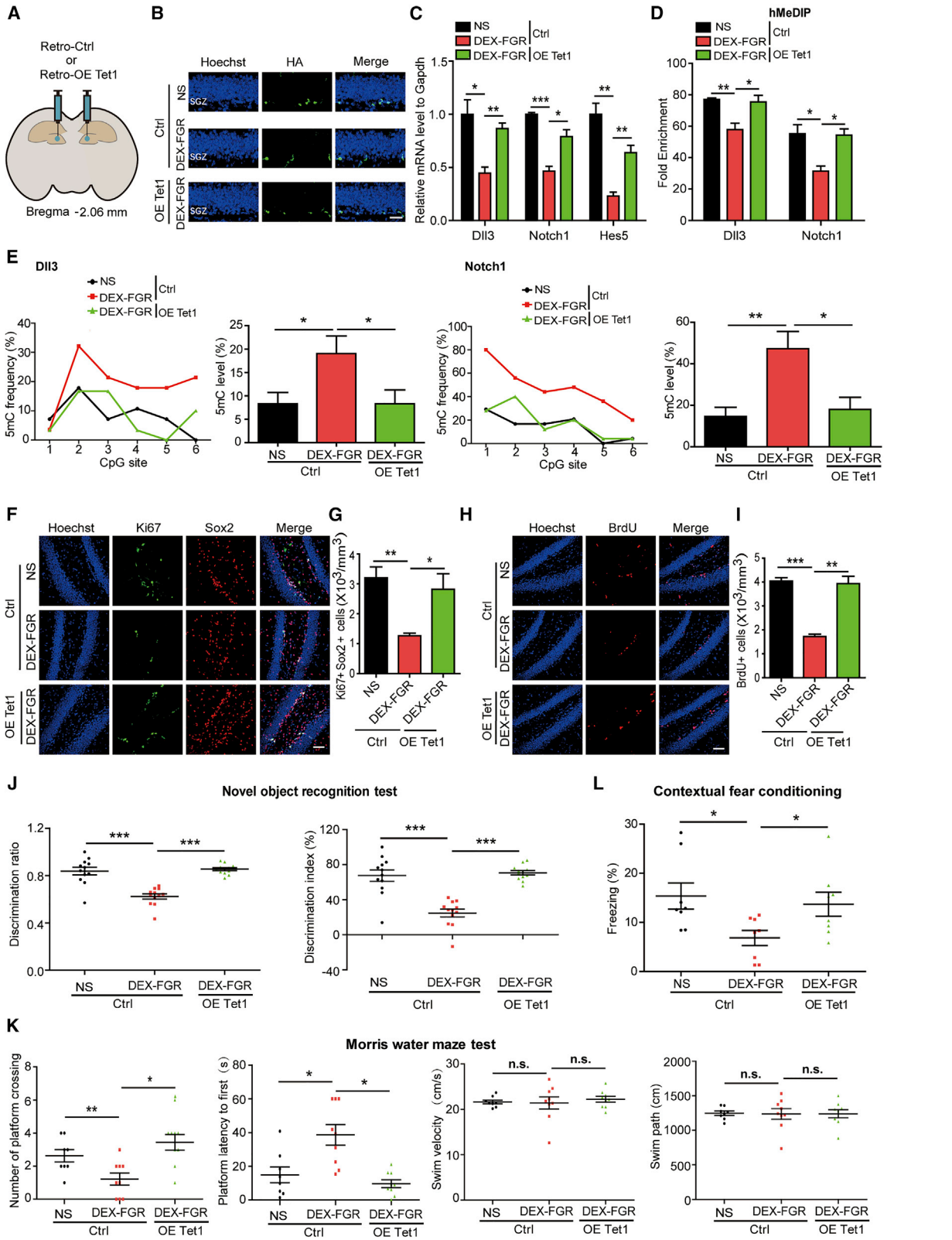

(legend on next page)

the epigenetic profile may partly explain the long-lasting DNA methylation state. Although all three Tet homologs can oxidize 5mC to 5hmC *in vitro*, their expression in multiple tissues and at different developmental stages appears to be variable (Wu and Zhang, 2011). A previous study in rat embryonic cortical NSCs indicated that DEX-induced DNA hypomethylation is associated with the upregulation of Tet3 (Bose et al., 2015). Our findings in post-natal mouse hippocampal NSCs showed that decreased Tet1 mediates DEX-induced alterations in 5hmC, the expression of downstream genes, and cell proliferation. Furthermore, it has been shown that only Tet1 expression is decreased in the post-natal hippocampus, but not in the cortex of FGR offspring. These data demonstrated that the function of Tet proteins in mediating epigenetic regulation could be tissue/cell type specific. Previous studies demonstrated that Tet proteins possess both enzymatic and nonenzymatic activities in neural development (Guo et al., 2011; Kaas et al., 2013; Rudenko et al., 2013). In this study, our findings showed that Tet1 regulates the DEX effect on NSC proliferation through an enzymatic mechanism. Similarly, a previous study also described that the loss of Tet1 in adult NSCs results in hypermethylation at the promoters of neurogenesis-related genes (Zhang et al., 2013). Recently, vitamin C was found to act as a cofactor to enhance the activity of Tet enzymes and promote DNA demethylation (Blaschke et al., 2013). Previous studies reported that vitamin C levels are lower in women who develop FGR during their pregnancy, and vitamin C supplementation in growth-restricted rats slightly increases fetal weight (Cohen et al., 2015; Ornoy et al., 2009). In the future, it would be of interest to explore the epigenetic roles of vitamin C in regulating the neurodevelopmental pathology of FGR.

Notch signaling, a highly conserved pathway, is necessary to maintain the NSC pool and hippocampal neurogenesis (Gonçalves et al., 2016). Previous studies demonstrated that its receptor Notch1 and essential effector Hes5 can promote NSC proliferation (Ehm et al., 2010; Ohtsuka et al., 2001). Our data indicated that the Notch ligand Dll3 positively regulates Notch1 and Hes5 expression and maintains NSC proliferation. Consistent with our results, a recent report showed that Dll3 downregulation attenuates Notch1 expression in human small-cell lung cancer cells (Furuta et al., 2019). Moreover, Dll3 is required for the normal expression of genes responsive to Notch signaling (Hes5, Hes1, and Hey1) in mouse presomitic mesoderm (Dunwoodie et al., 2002). Although some studies have revealed that Notch signaling can be regulated by DEX in differentiated cells (Cialfi et al., 2013; Hu et al., 2018), evidence of its regulation in stem cells is limited. Our findings indicated that DEX induced decreases in the expression of Notch signaling constituents (Dll3, Notch1, and Hes5) to inhibit the proliferation of hippocampal NSCs. Enrichment of 5hmC has been reported at Notch ligand and receptor genes in some tissues, but the mechanism and functional significance of this modification has not been examined (Terragni et al., 2014). In this study, we discovered a novel role of Tet1 in DEX-regulated Notch signaling. Following the classical molecular mechanism of Tet1-mediated transcriptional activation (Guo et al., 2011), we demonstrated that Tet1 binds directly to the Dll3 and Notch1 promoters and catalyzes 5mC hydroxylation to 5hmC in promoter CpG islands. Reducing Tet1 expression induces hypermethylation of Notch signaling genes, inhibits transcriptional activation, and ultimately blocks the proliferation of NSCs. In line with the *in vitro* findings, we further provided direct evidence that Tet1 overexpression in the hippocampal DGs of FGR offspring activates Notch signaling, offsets the decreased neurogenesis, and ameliorates learning and memory deficits. Although Tet1 protein lacks DNA-binding specificity, a recent study with mouse frontal cortex neurons showed that Tet1 achieves locus-specific demethylation via interaction with the transcription factor EGR1 and activates the expression of EGR1 downstream genes (Sun et al., 2019). By analyzing public ChIP-seq data, we found that Notch signaling genes in our study were not co-occupied by EGR1 and Tet1 in the frontal cortex. It would be interesting to identify specific proteins associated with Tet1 in the FGR hippocampus in the future.

In summary, our current work reveals that persistently decreased Tet1 expression in hippocampal NSCs from FGR offspring induces lasting DNA methylation changes in the promoters of Notch signaling genes and leads to the inhibition of Notch signaling; this in turn contributes to a sustained decrease in neurogenesis and impaired learning and memory in FGR offspring. Our findings expand the evidence of FGR-mediated epigenetic instability with regard to the risk of developing disease later in life and provide potential new targets for improving the long-term cognitive outcomes of FGR.

Limitations of the study

In this paper, we utilized the DEX model and the PR model for FGR. Considering these two models cannot recapitulate the entire FGR, the generalizability may be limited. Our study

Figure 6. Overexpression of Tet1 activates Notch signaling and ameliorates the neurogenic and behavioral abnormalities in DEX-FGR mice

(A) Schematic of retrovirus injection into the hippocampal DGs of NS and DEX-FGR mice.

(B) Immunostaining for HA in hippocampal DGs of NS mice injected with HA-Luc virus (Ctrl) and DEX-FGR mice injected with Ctrl virus or HA-Tet1 virus (OE Tet1). Scale bar, 50 μm.

(C) qPCR analysis of Dll3, Notch1, and Hes5 expression levels in the hippocampal DGs of the three groups (NS+Ctrl, DEX-FGR+Ctrl, and DEX-FGR+OE Tet1; n = 3).

(D) hMeDIP-qPCR analysis of 5hmC level changes at the promoters of Dll3 and Notch1 in the three groups (n = 3).

(E) Bisulfite sequencing analysis of CpG methylation status at Dll3 and Notch1 promoters in the three groups (n = 3).

(F and G) Immunostaining (F) and quantification of $Ki67^{+}Sox2^{+}$ cells (G) in the hippocampal DGs of the three groups (n = 3). Scale bar, 50 μm.

(H and I) Immunostaining (H) and quantification of $BrdU^{+}$ cells (I) in the hippocampal DGs of the three groups (n = 3). Scale bar, 50 μm.

(J and K) Increasing Tet1 in the hippocampi of DEX-FGR mice rescued the impaired learning and memory abilities by the novel object recognition test (J; n = 12) and the Morris water maze test (K; NS+Ctrl, n = 8; DEX-FGR+Ctrl, n = 9; DEX-FGR+OE Tet1, n = 9).

(L) Increasing Tet1 in the hippocampi of DEX-FGR mice rescued the impaired contextual memory (n = 8).

The data are shown as mean ± SEM. Two-tailed Student's t test, *p < 0.05, **p < 0.01, ***p < 0.001. SGZ, subgranular zone.

revealed that reducing Tet1 inhibited Notch signaling genes in the FGR hippocampus. However, the mechanism upstream of Tet1 remains to be uncovered.

STAR★METHODS

Detailed methods are provided in the online version of this paper and include the following:

- KEY RESOURCES TABLE
- RESOURCE AVAILABILITY
  - Lead contact
  - Materials availability
  - Data and code availability
- EXPERIMENTAL MODEL AND SUBJECT DETAILS
  - Experimental animals
  - Isolation of hippocampal NSCs
  - Plasmids
- METHOD DETAILS
  - Novel object recognition test
  - Morris water maze test
  - Open field test
  - Black/white box test
  - Contextual and auditory fear conditioning test
  - Hippocampus volume calculation
  - Cortisol analysis
  - BrdU pulse labeling and TUNEL Staining
  - Immunostaining
  - Fluorescence-activated cell sorting (FACS) analysis
  - Lentiviral and retroviral packaging
  - Lentiviral infection
  - Stereotaxic injections
  - RNA extraction, cDNA synthesis and Real-time quantitative PCR (qPCR)
  - RNA-sequencing (RNA-seq) analysis
  - Western blotting (WB)
  - Chromatin immunoprecipitation (ChIP)
  - Hydroxymethylated DNA immunoprecipitation (hMeDIP)
  - Methylation-specific PCR and bisulfite sequencing
  - Quantification of hydroxymethylated DNA levels
- QUANTIFICATION AND STATISTICAL ANALYSIS

SUPPLEMENTAL INFORMATION

Supplemental information can be found online at https://doi.org/10.1016/j.celrep.2021.109912.

ACKNOWLEDGMENTS

We thank Dandan Yang and Zhengliang Gao (Tongji University, China) for help with some technical aspects of the research. This work was supported by grants obtained from the National Natural Science Foundation of China (grants 82071728, 31830059, 31871495, 31970599, and 31721003).

AUTHOR CONTRIBUTIONS

W.C. and N.L. planned and performed experiments, analyzed data, and wrote the manuscript. S.S. analyzed the RNA-seq data. W.Z., J.Q., S.C., J.D., M.B., L.M., and S.W. performed experiments and collected the data. W.J., X.G., A.L., J.X., and C.J. contributed reagents and analysis tools and designed the experiments. J.K. designed and conceived this project, provided financial support, and approved the manuscript.

DECLARATION OF INTERESTS

The authors declare no competing interests.

Received: March 16, 2021
Revised: August 22, 2021
Accepted: October 9, 2021
Published: November 2, 2021

REFERENCES

Abul, M., Al-Bader, M.D., and Mouihate, A. (2019). Exposure to synthetic glucocorticoids during pregnancy alters the expression of p73 gene variants in fetal brains in a sex-specific manner. Brain Res. *1707*, 117–123.

Blaschke, K., Ebata, K.T., Karimi, M.M., Zepeda-Martínez, J.A., Goyal, P., Mahapatra, S., Tam, A., Laird, D.J., Hirst, M., Rao, A., et al. (2013). Vitamin C induces Tet-dependent DNA demethylation and a blastocyst-like state in ES cells. Nature *500*, 222–226.

Bose, R., Moors, M., Tofighi, R., Cascante, A., Hermanson, O., and Ceccatelli, S. (2010). Glucocorticoids induce long-lasting effects in neural stem cells resulting in senescence-related alterations. Cell Death Dis. *1*, e92.

Bose, R., Spulber, S., Kilian, P., Heldring, N., Lönnerberg, P., Johnsson, A., Conti, M., Hermanson, O., and Ceccatelli, S. (2015). Tet3 mediates stable glucocorticoid-induced alterations in DNA methylation and Dnmt3a/Dkk1 expression in neural progenitors. Cell Death Dis. *6*, e1793.

Cialfi, S., Palermo, R., Manca, S., Checquolo, S., Bellavia, D., Pelullo, M., Quaranta, R., Dominici, C., Gulino, A., Screpanti, I., and Talora, C. (2013). Glucocorticoid sensitivity of T-cell lymphoblastic leukemia/lymphoma is associated with glucocorticoid receptor-mediated inhibition of Notch1 expression. Leukemia *27*, 485–488.

Cohen, J.M., Beddaoui, M., Kramer, M.S., Platt, R.W., Basso, O., and Kahn, S.R. (2015). Maternal Antioxidant Levels in Pregnancy and Risk of Preeclampsia and Small for Gestational Age Birth: A Systematic Review and Meta-Analysis. PLoS ONE *10*, e0135192.

Costa, R.M., Honjo, T., and Silva, A.J. (2003). Learning and memory deficits in Notch mutant mice. Curr. Biol. *13*, 1348–1354.

Dieni, S., and Rees, S. (2003). Dendritic morphology is altered in hippocampal neurons following prenatal compromise. J. Neurobiol. *55*, 41–52.

Ding, Y.X., and Cui, H. (2017). Integrated analysis of genome-wide DNA methylation and gene expression data provide a regulatory network in intrauterine growth restriction. Life Sci. *179*, 60–65.

Dunwoodie, S.L., Clements, M., Sparrow, D.B., Sa, X., Conlon, R.A., and Beddington, R.S. (2002). Axial skeletal defects caused by mutation in the spondylocostal dysplasia/pudgy gene Dll3 are associated with disruption of the segmentation clock within the presomitic mesoderm. Development *129*, 1795–1806.

Edmonds, C.J., Isaacs, E.B., Cole, T.J., Rogers, M.H., Lanigan, J., Singhal, A., Birbara, T., Gringras, P., Denton, J., and Lucas, A. (2010). The effect of intrauterine growth on verbal IQ scores in childhood: a study of monozygotic twins. Pediatrics *126*, e1095–e1101.

Ehm, O., Göritz, C., Covic, M., Schäffner, I., Schwarz, T.J., Karaca, E., Kempkes, B., Kremmer, E., Pfrieger, F.W., Espinosa, L., et al. (2010). RBPJkappa-dependent signaling is essential for long-term maintenance of neural stem cells in the adult hippocampus. J. Neurosci. *30*, 13794–13807.

Fan, J., Zhang, Y., Mu, J., He, X., Shao, B., Zhou, D., Peng, W., Tang, J., Jiang, Y., Ren, G., and Xiang, T. (2018). TET1 exerts its anti-tumor functions via demethylating DACT2 and SFRP2 to antagonize Wnt/β-catenin signaling pathway in nasopharyngeal carcinoma cells. Clin. Epigenetics *10*, 103.

Furuta, M., Kikuchi, H., Shoji, T., Takashima, Y., Kikuchi, E., Kikuchi, J., Kinoshita, I., Dosaka-Akita, H., and Sakakibara-Konishi, J. (2019). DLL3

regulates the migration and invasion of small cell lung cancer by modulating Snail. Cancer Sci. *110*, 1599–1608.

Geva, R., Eshel, R., Leitner, Y., Valevski, A.F., and Harel, S. (2006). Neuropsychological outcome of children with intrauterine growth restriction: a 9-year prospective study. Pediatrics *118*, 91–100.

Gilchrist, C., Cumberland, A., Walker, D., and Tolcos, M. (2018). Intrauterine growth restriction and development of the hippocampus: implications for learning and memory in children and adolescents. Lancet Child Adolesc. Health *2*, 755–764.

Gonçalves, J.T., Schafer, S.T., and Gage, F.H. (2016). Adult Neurogenesis in the Hippocampus: From Stem Cells to Behavior. Cell *167*, 897–914.

Gontier, G., Iyer, M., Shea, J.M., Bieri, G., Wheatley, E.G., Ramalho-Santos, M., and Villeda, S.A. (2018). Tet2 Rescues Age-Related Regenerative Decline and Enhances Cognitive Function in the Adult Mouse Brain. Cell Rep. *22*, 1974–1981.

Good, C.R., Panjarian, S., Kelly, A.D., Madzo, J., Patel, B., Jelinek, J., and Issa, J.J. (2018). TET1-Mediated Hypomethylation Activates Oncogenic Signaling in Triple-Negative Breast Cancer. Cancer Res. *78*, 4126–4137.

Gundersen, H.J., and Jensen, E.B. (1987). The efficiency of systematic sampling in stereology and its prediction. J. Microsc. *147*, 229–263.

Guo, J.U., Su, Y., Zhong, C., Ming, G.L., and Song, H. (2011). Hydroxylation of 5-methylcytosine by TET1 promotes active DNA demethylation in the adult brain. Cell *145*, 423–434.

Herrero, A.I., Sandi, C., and Venero, C. (2006). Individual differences in anxiety trait are related to spatial learning abilities and hippocampal expression of mineralocorticoid receptors. Neurobiol. Learn. Mem. *86*, 150–159.

Hillman, S.L., Finer, S., Smart, M.C., Mathews, C., Lowe, R., Rakyan, V.K., Hitman, G.A., and Williams, D.J. (2015). Novel DNA methylation profiles associated with key gene regulation and transcription pathways in blood and placenta of growth-restricted neonates. Epigenetics *10*, 50–61.

Hu, C., Li, Z., Feng, J., Tang, Y., Qin, L., Hu, X., Zhang, Y., and He, R. (2018). Glucocorticoids Modulate Th1 and Th2 Responses in Asthmatic Mouse Models by Inhibition of Notch1 Signaling. Int. Arch. Allergy Immunol. *175*, 44–52.

Illa, M., Eixarch, E., Batalle, D., Arbat-Plana, A., Muñoz-Moreno, E., Figueras, F., and Gratacos, E. (2013). Long-term functional outcomes and correlation with regional brain connectivity by MRI diffusion tractography metrics in a near-term rabbit model of intrauterine growth restriction. PLoS ONE *8*, e76453.

Jaenisch, R., and Bird, A. (2003). Epigenetic regulation of gene expression: how the genome integrates intrinsic and environmental signals. Nat. Genet. *33* (*Suppl*), 245–254.

Kaas, G.A., Zhong, C., Eason, D.E., Ross, D.L., Vachhani, R.V., Ming, G.L., King, J.R., Song, H., and Sweatt, J.D. (2013). TET1 controls CNS 5-methylcytosine hydroxylation, active DNA demethylation, gene transcription, and memory formation. Neuron *79*, 1086–1093.

Kim, J.B., Ju, J.Y., Kim, J.H., Kim, T.Y., Yang, B.H., Lee, Y.S., and Son, H. (2004). Dexamethasone inhibits proliferation of adult hippocampal neurogenesis in vivo and in vitro. Brain Res. *1027*, 1–10.

LeDoux, J.E. (2000). Emotion circuits in the brain. Annu. Rev. Neurosci. *23*, 155–184.

Leitner, Y., Heldman, D., Harel, S., and Pick, C.G. (2005). Deficits in spatial orientation of children with intrauterine growth retardation. Brain Res. Bull. *67*, 13–18.

Lesage, J., Blondeau, B., Grino, M., Bréant, B., and Dupouy, J.P. (2001). Maternal undernutrition during late gestation induces fetal overexposure to glucocorticoids and intrauterine growth retardation, and disturbs the hypothalamo-pituitary adrenal axis in the newborn rat. Endocrinology *142*, 1692–1702.

Liu, J., Wang, H.W., Liu, F., and Wang, X.F. (2015). Antenatal taurine improves neuronal regeneration in fetal rats with intrauterine growth restriction by inhibiting the Rho-ROCK signal pathway. Metab. Brain Dis. *30*, 67–73.

Lodygensky, G.A., Seghier, M.L., Warfield, S.K., Tolsa, C.B., Sizonenko, S., Lazeyras, F., and Hüppi, P.S. (2008). Intrauterine growth restriction affects the preterm infant's hippocampus. Pediatr. Res. *63*, 438–443.

Maccari, S., Krugers, H.J., Morley-Fletcher, S., Szyf, M., and Brunton, P.J. (2014). The consequences of early-life adversity: neurobiological, behavioural and epigenetic adaptations. J. Neuroendocrinol. *26*, 707–723.

Mallard, E.C., Rehn, A., Rees, S., Tolcos, M., and Copolov, D. (1999). Ventriculomegaly and reduced hippocampal volume following intrauterine growth-restriction: implications for the aetiology of schizophrenia. Schizophr. Res. *40*, 11–21.

Mallard, C., Loeliger, M., Copolov, D., and Rees, S. (2000). Reduced number of neurons in the hippocampus and the cerebellum in the postnatal guinea-pig following intrauterine growth-restriction. Neuroscience *100*, 327–333.

Mandruzzato, G., Antsaklis, A., Botet, F., Chervenak, F.A., Figueras, F., Grunebaum, A., Puerto, B., Skupski, D., and Stanojevic, M.; WAPM (2008). Intrauterine restriction (IUGR). J. Perinat. Med. *36*, 277–281.

Ming, G.L., and Song, H. (2011). Adult neurogenesis in the mammalian brain: significant answers and significant questions. Neuron *70*, 687–702.

Moors, M., Bose, R., Johansson-Haque, K., Edoff, K., Okret, S., and Ceccatelli, S. (2012). Dickkopf 1 mediates glucocorticoid-induced changes in human neural progenitor cell proliferation and differentiation. Toxicol. Sci. *125*, 488–495.

Neri, F., Dettori, D., Incarnato, D., Krepelova, A., Rapelli, S., Maldotti, M., Parlato, C., Paliogiannis, P., and Oliviero, S. (2015). TET1 is a tumour suppressor that inhibits colon cancer growth by derepressing inhibitors of the WNT pathway. Oncogene *34*, 4168–4176.

Ohtsuka, T., Sakamoto, M., Guillemot, F., and Kageyama, R. (2001). Roles of the basic helix-loop-helix genes Hes1 and Hes5 in expansion of neural stem cells of the developing brain. J. Biol. Chem. *276*, 30467–30474.

Ornoy, A., Tsadok, M.A., Yaffe, P., and Zangen, S.W. (2009). The Cohen diabetic rat as a model for fetal growth restriction: vitamins C and E reduce fetal oxidative stress but do not restore normal growth. Reprod. Toxicol. *28*, 521–529.

Rudenko, A., Dawlaty, M.M., Seo, J., Cheng, A.W., Meng, J., Le, T., Faull, K.F., Jaenisch, R., and Tsai, L.H. (2013). Tet1 is critical for neuronal activity-regulated gene expression and memory extinction. Neuron *79*, 1109–1122.

Song, J., Sun, J., Moss, J., Wen, Z., Sun, G.J., Hsu, D., Zhong, C., Davoudi, H., Christian, K.M., Toni, N., et al. (2013). Parvalbumin interneurons mediate neuronal circuitry-neurogenesis coupling in the adult hippocampus. Nat. Neurosci. *16*, 1728–1730.

Sun, Z., Xu, X., He, J., Murray, A., Sun, M.A., Wei, X., Wang, X., McCoig, E., Xie, E., Jiang, X., et al. (2019). EGR1 recruits TET1 to shape the brain methylome during development and upon neuronal activity. Nat. Commun. *10*, 3892.

Swanson, A.M., and David, A.L. (2015). Animal models of fetal growth restriction: Considerations for translational medicine. Placenta *36*, 623–630.

Szulwach, K.E., Li, X., Li, Y., Song, C.X., Wu, H., Dai, Q., Irier, H., Upadhyay, A.K., Gearing, M., Levey, A.I., et al. (2011). 5-hmC-mediated epigenetic dynamics during postnatal neurodevelopment and aging. Nat. Neurosci. *14*, 1607–1616.

Tan, C.K., Yan, J., Ananth, C., and Kaur, C. (2002). Dexamethasone induces dendritic alteration but not apoptosis in the neurons of the hippocampus in postnatal rats. Neurosci. Lett. *326*, 206–210.

Terragni, J., Zhang, G., Sun, Z., Pradhan, S., Song, L., Crawford, G.E., Lacey, M., and Ehrlich, M. (2014). Notch signaling genes: myogenic DNA hypomethylation and 5-hydroxymethylcytosine. Epigenetics *9*, 842–850.

Wu, H., and Zhang, Y. (2011). Mechanisms and functions of Tet protein-mediated 5-methylcytosine oxidation. Genes Dev. *25*, 2436–2452.

Zhang, R.R., Cui, Q.Y., Murai, K., Lim, Y.C., Smith, Z.D., Jin, S., Ye, P., Rosa, L., Lee, Y.K., Wu, H.P., et al. (2013). Tet1 regulates adult hippocampal neurogenesis and cognition. Cell Stem Cell *13*, 237–245.

STAR★METHODS

KEY RESOURCES TABLE

REAGENT or RESOURCE	SOURCE	IDENTIFIER
Antibodies		
Rabbit polyclonal to anti-Ki67	Abcam	Cat# ab15580; RRID: AB_443209
Goat polyclonal to anti-SOX2	R&D Systems	Cat# AF2018; RRID: AB_ 355110
Rat monoclonal to anti-BrdU	Abcam	Cat# ab6326; RRID: AB_ 305426
Mouse monoclonal to anti-BrdU	Bioworld	Cat# MB6004
Rabbit polyclonal to anti-NeuN	Millipore	Cat# ABN78; RRID: AB_ 10807945
Mouse monoclonal to anti-S100β	Abcam	Cat# ab11178; RRID: AB_ 297817
Rabbit polyclonal to anti-Dll3	Novus Biologicals	Cat# NBP2-24669
Rabbit monoclonal to anti-N1ICD	Cell Signaling Technology	Cat# 4147s; RRID: AB_2153348
Rabbit polyclonal to anti-Hes5	ABclonal	Cat# A16237; RRID: AB_2769766
Rabbit polyclonal to anti-Tet1	GeneTex	Cat# GTX124207; RRID: AB_11176491
Mouse monoclonal to anti-Tet1	GeneTex	Cat# GTX627420; RRID: AB_11172316
Rabbit polyclonal to anti-Tet2	GeneTex	Cat# GTX124205; RRID: AB_11166461
Rabbit polyclonal to anti-Tet2	ABclonal	Cat# A5682; RRID: AB_2766442
Rabbit polyclonal to anti-Tet3	GeneTex	Cat# GTX121453; RRID: AB_10723106
Rabbit polyclonal to anti-Tet3	ABclonal	Cat# A7612; RRID: AB_ 2768131
Rabbit polyclonal to anti-Dnmt1	Santa Cruz	Cat# SC-20701; RRID: AB_2293064
Mouse monoclonal to anti-Dnmt1	Santa Cruz	Cat# SC-52919; RRID: AB_ 783092
Rabbit polyclonal to anti-Dnmt3a	Cell Signaling Technology	Cat# 2160s; RRID: AB_2263617
Rabbit monoclonal to anti-Dnmt3a	Cell Signaling Technology	Cat# 3598s; RRID: AB_2277449
Rabbit polyclonal to anti-Dnmt3b	Santa Cruz	Cat# sc-20704; RRID: AB_ 2094125
Rabbit polyclonal to anti-Dnmt3b	Abcam	Cat# ab2851; RRID: AB_303356
Rabbit polyclonal to anti-HA	Abcam	Cat# ab9110; RRID: AB_ 307019
Rabbit monoclonal to anti-HA	Cell Signaling Technology	Cat# 5017s; RRID: AB_10693385
Rabbit polyclonal to anti-GAPDH	Bioworld	Cat# AP0063; RRID: AB_ 2651132
Rabbit polyclonal to anti-5hmC	Active Motif	Cat# 39769; RRID: AB_10013602
Alexa Fluor 488 Donkey Anti-Mouse	Invitrogen	Cat# A-21202; RRID: AB_141607
Alexa Fluor 488 Donkey Anti-Rabbit	Invitrogen	Cat# A-21206; RRID: AB_14170
Alexa Fluor 594 Donkey Anti-Rat	Invitrogen	Cat# A-21209; RRID: AB_ 2535795
Alexa Fluor 594 Donkey Anti-Goat	Invitrogen	Cat# A-11058;RRID: AB_142540
Rat IgG2a kappa Isotype Control (eBR2a), eFluor 660	Thermo Fisher Scientific	Cat#50-4321-82; RRID: AB_ 10598503
SOX2 Monoclonal Antibody (Btjce), eFluor 660	Thermo Fisher Scientific	Cat#50-9811-82;RRID: AB_ 11220483
Bacterial and virus strains		
5-alpha Competent *E. coli*	TIANGEN	CB101
Chemicals, peptides, and recombinant proteins		
Dexamethasone	Selleck	Cat# S1322
DAPT	Selleck	Cat# S2215
BrdU	Sigma	Cat# B5002
Saponin	Sigma	Cat# 47036-50G-F
Lenti-concentin	ExCell Bio	Cat# EMB810A-1
Retro-concentin	ExCell Bio	Cat# EMB100A-1
Recombinant Human FGF-basic (bFGF)	Sino Biological	Cat# 10014-HNAE

(*Continued on next page*)

Continued

REAGENT or RESOURCE	SOURCE	IDENTIFIER
Recombinant Human EGF	Sino Biological	Cat# 10605- HNAE
Hibernate™-A medium	Invitrogen	Cat# A1247501
Red blood cell lysis buffer	Biogems	Cat# 64010-00-100
Critical commercial assays		
PrimeScript™ RT reagent Kit	Takara	Cat# RR037A
Takara Ex Taq PCR kit	Takara	Cat# RR420A
TACS® 2 TdT Fluorescein Kit	Trevigen	Cat# 4812-30-K
KOD DNA Polymerase	Genview	Cat# GK1101
QuikChange XL Site-Directed Mutagenesis Kit	Stratagene	Cat# 200516
DNA extraction kit	QIAGEN	Cat# 69504
MinElute PCR Purification kit	QIAGEN	Cat# 28004
Neural Tissue Dissociation Kit	Miltenyi Biotec	Cat#130-092-628
Mouse Cortisol ELISA Kit	J&L Biological	Cat# JL12086
Nissel staining	Solarbio	Cat# G1436
Deposited data		
RNA-seq data	This manuscript	GSE143816
5-hmC data	Szulwach et al., 2011	GSE32050
RNA-seq data	Rudenko et al., 2013	GSE48789
ChIP-seq data	Sun et al., 2019	GSE108768
All original data	This manuscript	Mendeley https://doi.org/10.17632/s7223s5gpt.2
Experimental models: Cell lines		
The primary mouse hippocampal neural stem cells (NSCs)	This manuscript	N/A
Experimental models: Organisms/strains		
C57BL/6J	Shanghai SLAC Laboratory Animal Co. Ltd	N/A
Oligonucleotides		
Primers used for qPCR、vetor construction、ChIP-qPCR、hMeDIP-qPCR、Bisulfite Assay,See Table S2	This manuscript	N/A
Recombinant DNA		
pLKO.1	Addgene	Cat# 8453; RRID: AB_8453
pLKO.1-shCtrl	This manuscript	N/A
pLKO.1-shTet1-1/-2	This manuscript	N/A
pLKO.1-shDll3-1/-2	This manuscript	N/A
FUGW	Addgene	Cat# 14883; RRID: AB_14883
FUGW-HA-Luc	This manuscript	N/A
FUGW-HA-Tet1	This manuscript	N/A
FUGW-HA-Tet1 mutant	This manuscript	N/A
FUGW-HA-N1ICD	This manuscript	N/A
pMXs	Addgene	Cat# 13367; RRID: AB_13367
pMXs-HA-Luc	This manuscript	N/A
pMXs-HA-Tet1	This manuscript	N/A

(*Continued on next page*)

Continued

REAGENT or RESOURCE	SOURCE	IDENTIFIER
Software and algorithms		
GraphPad Prism 5	GraphPad Software	https://www.graphpad.com/support/faqid/1952/
ImageJ	NIH	https://imagej.nih.gov/ij/download.html
FlowJo	Ashland	https://www.flowjo.com/solutions/flowjo/downloads
R version 3.6.0	The R Foundation for Statistical Computing	https://www.r-project.org/

RESOURCE AVAILABILITY

Lead contact

Further information and requests for resources and reagents should be directed to and will be fulfilled by the Lead Contact, Jiuhong Kang (jhkang@tongji.edu.cn).

Materials availability

Plasmids and cell lines generated in this study are available upon request.

Data and code availability

- The accession number for the RNA-seq reported in this paper is GEO: GSE143816. The public data including the profiling of 5-hmC in mouse hippocampus, the RNA-seq dataset of the hippocampus of Tet1 KO mice, and the ChIP-seq dataset from the frontal cortex of Egr1 KO and Tet1 KO mice were analyzed during this study. The accession codes are GEO: GSE32050, GEO: GSE48789 and GEO: GSE108768. All original data has been deposited at Mendeley and is publicly available as of the date of publication. The DOI is listed in the Key resources table.
- This paper does not report original code.
- Any additional information required to reanalyze the data reported in this work paper is available from the Lead Contact upon request.

EXPERIMENTAL MODEL AND SUBJECT DETAILS

Experimental animals

The mice (C57BL/6J) used in this study were purchased from SLAC Laboratory Animal Company (Shanghai, China). Mice were housed under pathogen-free conditions, maintained in a temperature- and humidity-controlled room with a 12 hours light/12 hours dark cycle. C57BL/6J virgin female mice were mated with male mice. Mice with pregnancy confirmed by the presence of a vaginal plug next morning, which was designated as 0.5 days post coitus (dpc). Two maternal mouse models aimed at inducing FGR during pregnancy were used: prenatal overexposure to DEX or consumption of a protein restriction (PR) diet. In the DEX overexposure model, pregnant mice were assigned randomly to the DEX group or normal saline (NS) group. The pregnant mice in the DEX group were intraperitoneally injected with DEX (1 mg/kg/d, Selleck, S1322) at 14.5 dpc for five consecutive days; the mice in the NS group received the same volume of NS on the same schedule. In the prenatal PR diet model, pregnant mice at 0.5 dpc were individually housed and fed a standard normal chow diet (NC; 20% protein) or a PR diet (8% protein) until labor. In both two mouse models, the newborn pups were kept with their mothers until weaning. After weaning, pups of a single sex were housed in groups of 4 to 5 animals in the same environment until grown-up. Male mouse offspring were used in all experiments, adult male mice at 8 to 12 weeks of age were used in the following behavioral tests. All behavioral experiments were performed during the light phase of the light/dark cycle. The experimenter was blind to the group identity of the tested mice. Procedures were designed to minimize the number of animals used and their suffering. Animal handling and experimental procedures were approved by the Institutional Animal Care and Use Committee of Tongji University (TJAB04520101).

Isolation of hippocampal NSCs

Hippocampal NSCs were isolated from the male C57BL/6J mice at post-natal day 3 and 8- week according to neural tissue dissociation kit (P, Miltenyi Biotec). NSCs were cultured in the DMEM/F12 (GIBCO) supplemented with 2% B27 supplement without

vitamin A (Invitrogen), 1% GlutaMAX (Invitrogen), 1% NEAA (Invitrogen), 20 ng/ml fibroblast growth factor (bFGF, Sino_Biological), and 20 ng/ml epidermal growth factor (EGF, Sino_Biological) at 37°C and 5% CO_2, with passaging every 4-5 days.

Plasmids

For gene knockdown plasmids, the corresponding short hairpin RNA (shRNA) nucleotides (Tet1 and Dll3) and non-targeting control shRNA were cloned into the AgeI and EcoRI sites of the pLKO.1 RNAi plasmid (Addgene plasmid # 8453). For gene overexpression plasmids, the cDNA sequences with HA (hemagglutinin) –tag of human Tet1 (GenBank:NM_030625.3, aa1418–2136) and N1ICD (GenBank:NM_008714.3, aa1753-2531) were isolated using KOD DNA polymerase (Genview, GK1101). N1ICD was cloned into the FUGW lentiviral vector (Addgene plasmid # 14883). Tet1 was cloned into the FUGW lentiviral vector and pMXs retroviral vector (Addgene plasmid # 13367). The Tet1 mutant (H1671Y/D1673A) was generated by site-specific mutagenesis (Stratagene, QuikChange Kit, 200516). The plasmid encoding luciferase with HA-tag was constructed as a control vector. Sequences of the primers are shown in Table S2.

METHOD DETAILS

Novel object recognition test

Mice were placed into a black Plexiglas rectangular chamber (25 cm length × 25 cm width × 25 cm height). Each mouse was gently placed in the box with two same objects (a white round object) located diagonally, and allowed to explore freely for 20 minutes every day for three consecutive days, then sent back to their home cage. After 24 hours, the mice were placed back to the box (with one object changed to a white square object) again for 5 minutes for retention test. Exploration of the objects was defined as sniffing of the objects (with nose contact or head directed toward the object) within a 2-cm radius of the objects. Sitting or standing on the objects was not scored as exploration. The discrimination index = (novel-object exploration time – familiar-object exploration time) / total exploration time × 100. The discrimination ratio = novel-object exploration time /total exploration time.

Morris water maze test

Mice were handled for 5 minutes daily for 1 week before swim training. The test used a 1.2-m diameter circular blue pool, which was divided into four hypothetical, equal quadrants. A platform (diameter: 10 cm) was placed 1 cm below the water surface in the middle of the target quadrant. On training days, mice were trained to find the hidden platform. Each trial started with a random point away from the visible platform and lasted either until the mouse had found the platform or for a maximum of 60 s. If a mouse did not reach the platform within 60 s, it was guided to the platform. When a mouse reached the platform within 60 s and stayed on the platform for more than 20 s, it was taken to the home-cage. Mice were trained with four trials per day with an intertrial interval of 1 minute for 5 consecutive days. On the 6th day, the platform was removed and each mouse was allowed 60 s to search the pool for the platform. Noldus software (EthoVision XT 8.0, Noldus Technology) was used to track the movement of mice. Latency to find the platform, frequency of platform crosses, average velocity and total distance traveled were measured automatically by the software.

Open field test

Mice were placed in the test room one hour to adapt environment before start experiment. Then each mouse was placed at the center of the chamber (27 cm length × 27 cm width × 20 cm height, Med Associates) for 6 minutes. After the mice adapted to the environment in the first 1 minute, the movements within the next 5 minutes were recorded by a computerized video-tracking system, and analyzed by Activity Monitor software.

Black/white box test

Mice were placed in the test room one hour to adapt environment. The apparatus was a rectangular plexiglass box (45 cm length × 30 cm width × 30 cm height) divided into a smaller (1/3) black area with a lid and a larger (2/3) white area with an open-top. A black wall separated the two compartments and had an opening door (5 cm width × 7.5 cm height) at floor level. Each mouse was placed in the white box and behavior was recorded over a 5-minute period. The time spent in the white box and the crossing numbers between dark and white compartments were recorded.

Contextual and auditory fear conditioning test

Before testing, mice were first habituated to the testing room for 1h. In the context-dependent fear conditioning training, mice were placed in a conditioning box and allowed to freely explore for 3 min before receiving a foot shock (2 s, 0.8 mA). The contextual fear memory test was performed 24 h later by re-introducing the mice into the conditioning box for 6 min without receiving any foot shocks. Freezing responses were recorded during the last 3 min. In the tone-dependent fear conditioning training, mice were placed in a conditioning box and allowed to freely explore for 3 min. At the end of 3 min, mice were subjected to an audio tone (30 s, 5 kHz, 75 dB), followed immediately by a 2 s, 0.8 mA foot shock. For auditory fear memory tests, mice were placed in a novel box to explore the chamber for 3 min following 3 min audio tones. Freezing responses were recorded during the last 3 min when the tone was delivered. FreezeFrame and FreezeView software systems (Coulbourn Instruments, USA) were used to record and analyze freezing behaviors.

Hippocampus volume calculation

After fixation with 4% PFA following equilibration with sucrose, brains were cut coronally into 50 μm sections from the anterior to the posterior direction. Every 5th section of 50 μm thick cuts was annotated resulting in 8 to 10 sections per hippocampus. All sections were used for Nissel staining (Solarbio, G1436) to trace the contours of the hippocampus. Images were acquired on a microscope system (Olympus, SZ2-ILST). Volume estimation was calculated according to the Cavalieri principle (Gundersen and Jensen., 1987) using the formula $V = t \times \sum a \times 2$. where V is the total volume, t is the section thickness with a sampling fraction of 1/5 (250 μm), $\sum a$ is the sum of the areas of the unilateral hippocampus measured by ImageJ software, and the factor 2 denotes the bilateral hippocampus.

Cortisol analysis

On day 18.5 of gestation and post-natal 3- week, blood samples were taken between 1000–1200 h to determine cortisol levels. All blood samples were collected in tubes precoated with EDTA-K2 and centrifuged at 1500 rpm for 10 min at 4°C. Aliquots of the supernatants were stored at −80°C until assayed. Cortisol plasma levels were determined using a mouse cortisol ELISA Kit (J&L Biological, JL12086) according to the manufacturer's instructions.

BrdU pulse labeling and TUNEL Staining

Mice received intraperitoneal injections of BrdU (5-Bromo-2′-deoxyuridine, Sigma, 50 mg/kg) once daily for 7 consecutive days. For NSC proliferation studies, brains were fixed the next day; for differentiation studies, brains were fixed 3 weeks later. Then brain sections were processed for immunostaining. Cell apoptosis in the mouse hippocampus was examined using a TACS 2 TdT-Fluor *in situ* apoptosis detection kit (Trevigen, 4812-30-K).

Immunostaining

For cell immunostaining, cells cultured on poly-O-lysine/laminin-coated glass coverslips were pretreated with BrdU (30 μM) for 4 hours. Then cells were fixed in 4% paraformaldehyde for 20 minutes, treated with 2 M HCl for 30 minutes, permeabilized with 0.2% Triton X-100/phosphate-buffered saline (PBS) for 8 minutes and blocked in 10% donkey serum in PBS for 1 hour. For brain immunostaining, mice were transcardially perfused with 4% PFA. Brains collected were cryoprotected in 20% sucrose/PBS for 24 hours, and then 30% sucrose/PBS for 24 hours. Coronal frozen slices at 35 μm thick were prepared on a freezing microtome (Leica CM3050 S) and stored in the brain freezing medium which contains 30% sucrose and 30% ethanediol, 11.36% Na2HPO4 and 2.4% NaH2PO4. After heat retrieval, sections were permeabilized and blocked with PBS containing 10% donkey serum and 0.1% Triton X-100 for 1 hour at room temperature. Brain sections for BrdU staining were treated with 2 M HCl for 1 hour at room temperature before permeabilization and blocking. Both cells and brain sections were incubated in primary antibody diluted in 10% donkey serum overnight at 4°C, washed, and incubated with Alexa Fluor secondary antibody (Invitrogen) for 2 hours. The following primary antibodies were used: Ki67 (1:1000, Abcam, ab15580), Sox2 (1:500, R&D Systems, AF2018), BrdU (1:1000, Bioworld, MB6003, for cell immunostaining), BrdU (1:1000, Abcam, ab6326, for tissue immunostaining), NeuN (1:1000, Millipore, ABN78), S100β (1:1000, Abcam, ab11178) and HA (1:1000, CST, 5017s). Coverslips were washed, stained with Hoechst and mounted. Images were acquired on a confocal laser microscope system (Nikon). For quantification, overlapping images of the entire DG on each section were captured by confocal microscopy in z stack. The density of cells was determined by dividing the total number of cells by the corresponding volume of hippocampal DG.

Fluorescence-activated cell sorting (FACS) analysis

The hippocampi were isolated and dissociated with the Neural Tissue Dissociation Kit P (Miltenyi Biotec, 130-092-628). The enzymatic digestion was diluted by adding 9 mL of Hibernate™-A medium (Invitrogen, A1247501), and the preparation was centrifuged at 250 × g for 8 min. Cell pellets were resuspended in 0.5 mL of 1×red blood cell lysis buffer (Biogems, 64010-00-100) and incubated for 1 min. Next, 5 mL of Hibernate™-A medium was added, and the preparation was centrifuged at 250 × g for 6 min. Isolated cells were fixed and permeabilized with fixation buffer containing 4% PFA and 0.1% saponin (Sigma, 47036) in PBS on ice for 30 min, washed once in PBS containing 0.2% BSA and 0.1% saponin, stained with primary antibodies diluted in blocking buffer (1% BSA, 0.1% saponin in PBS), and detected using fluorescent-tagged secondary antibodies. For Tet1 staining, Tet1 (1:500, GeneTex, GTX627420) and its isotype control, Alexa Fluor 488-conjugated donkey anti-mouse IgG (H+L; 1:500, Invitrogen, A-21202), were used. For Sox2 staining, eFluor 660-conjugated Sox2 antibody (1:200, Thermo Fisher Scientific, 50-9811-82) and its isotype control, eFluor 660-conjugated rat IgG2a kappa antibody (eBR2a) (1:200, Thermo Fisher Scientific, 50-4321-82) were used. Flow cytometry was performed on a BD FACSVerse flow cytometer. The data were analyzed using FlowJo software.

Lentiviral and retroviral packaging

For lentivirus packaging, pLKO.1 RNAi or FUGW plasmid (1.2 μg) was cotransfected with the packaging plasmids Pax2 (0.9 μg) and Vsvg (0.6 μg) into 293FT cells (1 well of a 6-well-plate) using the FuGENE HD transfection reagent (Roche). After 72 hours lentivirus-containing media was filtered to remove cellular debris, concentrated by lentivirus precipitation solution (ExCell Bio, EMB810A-1). Harvested lentiviral particles were suspended in 100 μl PBS for cell infection. For retrovirus packaging, pMXs plasmid (2 μg) was transfected into Plat-E cells (1 well of a 6-well-plate) using the FuGENE HD transfection reagent. After 72 hours retrovirus-containing

media was filtered to remove cellular debris, concentrated by retrovirus precipitation solution (ExCell Bio, EMB100A-1). Harvested retroviral particles were suspended in 2 μl PBS for brain injection.

Lentiviral infection

Hippocampal NSCs grown as neurospheres or plated on poly-O-lysine/laminin-coated cover glasses and exposed to DMSO (Sigma), DEX (50 μM, Selleck) or the Notch signaling pathway inhibitor DAPT (Selleck, S2215). For lentiviral infection, hippocampal NSCs were dissociated by TrypLE (Invitrogen) and suspensions were diluted to 2×10^5 cells per well in 6-well plates, and incubate with 20 μL lentiviruses for 48 hours; then, the medium was replaced with fresh NSC medium. In addition, to generate knockdown cells, 0.5 μg/ml puromycin (Sigma) was added 48 hours after infection.

Stereotaxic injections

Mice were anesthetized with Avertin (20 μl/g) (Aladdin, A103416) through intraperitoneal injection and placed in a stereotaxic frame. The area around the incision was trimmed, and then, treated the meninges with 3% hydrogen peroxide (Aladdin) and find the bregma to locate the origin. Solutions were injected bilaterally into the DG of the dorsal hippocampi using the following coordinates: (from bregma) anterior = −1.75 mm, lateral = ± 1.75 mm, (from skull surface) height = −2.06 mm. A 2.0 μl of concentrated retroviruses was injected stereotaxically over 10 minutes (injection speed: 0.20 μl/min) using a 5-μl 33 s-gauge Hamilton syringe. To prevent the virus from refluxing along the injection track, the needle was maintained *in situ* for 10 minutes, and slowly pulled out. The skin was closed using silk suture. Mice were singly housed and monitored during recovery. Behavioral tests were performed four-five weeks after viral injection.

RNA extraction, cDNA synthesis and Real-time quantitative PCR (qPCR)

Total RNA was isolated from the cells or tissues using RNAiso plus (Takara, 108-95-2). 0.5 μg of total RNA was reverse transcribed using PrimeScript™ RT reagent kit (TaKaRa, RR037A). qPCR was performed using the Takara Ex Taq PCR kit (TaKaRa, RR420A) in the Stratagene Mx3000 QPCR system (Stratagene). The results were calculated using the $2^{-\Delta\Delta ct}$ method by normalizing with *Gapdh* (glyceraldehyde-3-phosphate dehydrogenase) gene. Sequences of the primers used in this study are shown in Table S2.

RNA-sequencing (RNA-seq) analysis

RNA quality and quantity validation was conducted using an Agilent Bioanalyzer 2100 (Agilent Technologies). Library building and high-throughput sequencing were conducted by Beijing Genomics Institute. Low-quality and adaptor sequences were trimmed from the reads using Cutadapt (v1.16). Then, the reads were mapped to the mouse genome (mm10, obtained from UCSC) using Hisat2 (v2.1.0). Mapped reads were subsequently assembled into transcripts guided by the UCSC gff annotation files (mm10) using featureCounts (v1.6.1). The expression level of each gene was quantified and normalized by DEseq2 (v1.26.0) in R. The differentially expressed genes were also calculated by DEseq2(v1.26.0) in R. Among them, those P value less than 0.05 were used in the further analysis. Gene ontology analysis was performed using DAVID V6.8 (https://david.ncifcrf.gov/). Gene set enrichment analysis (GSEA) was performed using the GSEA platform (GSEA v3.0).

Western blotting (WB)

Tissue proteins were extracted from the whole hippocampi from NS and FGR mice at the PD3, and the hippocampal DGs from two groups at P3W and P8W. Cells or tissues were lysed in RIPA buffer (KeyGen, KGP703-100) with PMSF and HaltTM Protease Inhibitor Cocktails (Thermo), and the protein concentrations were measured using the Pierce BCA Protein Assay Kit (Thermo, 23228). Proteins were separated by SDS-PAGE and transferred onto PVDF membranes (Perkin Elmer Life Sciences). Primary antibodies were incubated overnight at 4°C, followed by incubation with the appropriate secondary antibodies. The following primary antibodies were used: Dll3 (1:1000, Novus, NBP2-24669), N1ICD (1:1000, CST, 4147S), Hes5 (1:1000, ABclonal, A16237), Tet1 (1:1000, GeneTex, GTX124207), Tet2 (1:1000, GeneTex, GTX124205; 1:500, ABclonal, A5682), Tet3 (1:1000, GeneTex, GTX121453; 1:1000, ABclonal, A7612), Dnmt1 (1:1000, Santa Cruz, SC-20701; 1:1000, Santa Cruz, SC-52919), Dnmt3a (1:1000, CST, 2160s; 1:1000, CST, 3598s), Dnmt3b (1:1000, Santa Cruz, SC-20704; 1:1000, Abcam, ab2851), HA (1:5000, Abcam, ab9110). Signals were detected using the SuperSignal West Pico Chemiluminescent Substrate (Pierce) and visualized by an imaging system (ImageQuant LAS 4000). Results were analyzed with Gel-Pro Analyzer 4.0 software (Media Cybernetics, USA) for quantification. Validation of antibody specificity by knockout/knockdown or overexpression from company websites and publications are shown in Table S3. The original entire blots and respective calculations of WB are shown in the Data S1 and Table S4.

Chromatin immunoprecipitation (ChIP)

1×10^7 hippocampal NSC cells were crosslinked with 1% formaldehyde for 10 minutes at room temperature, and quenched with 1.25 M glycine for 5 minutes. For the hippocampus, 50 mg tissues in 450 μL PBS were homogenized using 18G and 21G needles, then fixed with formaldehyde and quenched with glycine. Cells or tissues were washed with PBS three times and spun down at 1,500 r/min for 10 minutes. The cell pellets were resuspended in 500 μL Cell Lysis Buffer (5 mM PIPES pH 8.0, 85 mM KCl, and 0.5% NP40 and protease inhibitor cocktail) incubated on ice for 15 minutes, and centrifuged at 3,000 r/min for 5 minutes. Nuclear pellets were further lysed in 400 μL Nuclei Lysis Buffer (50 mM Tris pH 8.1, 10 mM EDTA, 0.75% SDS and protease inhibitor cocktail). Cell lysate

was sonicated for 10 minutes (peak power, 75; duty factor, 10; cycles/burst, 150) using a M220 Focused-ultrasonicator (Covaris) to generate DNA fragments of 500 to 1000 base pairs (bp). After sonication, nuclear lysate was cleared by centrifugation at 13,000 r/min for 10 minutes to keep supernatant. The nuclear lysate was diluted with 2 volumes of dilution buffer (16.7 mM Tris-HCl pH 8.1, 167 mM NaCl, 0.01% SDS, 1.2 mM EDTA and 1.1% Triton X-100 and protease inhibitor cocktail). The samples incubated with the following antibodies: 4 μg of Tet1 (GeneTex, GTX124207) and 4 μg of normal rabbit IgG (Invitrogen, a21206) overnight at 4°C. The immune complexes were precipitated with 20 μL ProteinG dynabeads (Invitrogen) for an additional 2 hours, and washed sequentially with a low-salt wash buffer (0.1% SDS, 1% Triton X-100, 2 mM EDTA, 20 mM Tris–HCl at pH 8.1 and 150 mM NaCl), a high-salt wash buffer (0.1% SDS, 1% Triton X-100, 2 mM EDTA, 20 mM Tris–HCl at pH 8.1 and 500 mM NaCl), an LiCl wash buffer (0.25 M LiCl, 1% NP-40, 1% deoxycholate, 1 mM EDTA and 10 mM Tris–HCl at pH 8.1) and TE buffer (10 mM Tris–HCl at pH 8.1 and 1 mM EDTA). Then the immunocomplexes were eluted in ChIP elution buffer (1% SDS and 0.1 M $NaHCO_3$) and the crosslinking was reversed overnight at 65°C. Samples were treated with Proteinase K and RNase A, followed by phenol/chloroform extraction and ethanol precipitation. Ten percent of the total genomic DNA from the nuclear extract was used as the input. Purified immunoprecipitated DNA and input DNA were used as a template for subsequent qPCR with the primers in Table S2.

Hydroxymethylated DNA immunoprecipitation (hMeDIP)

500 ng digested DNA was diluted to 178 μL in 1 × TE buffer (pH 8.0), and denatured by heating at 95°C for 10 minutes, followed by plunging the samples on ice for 10 minutes. Samples were divided into input and immunoprecipitation samples. Then, 20 μL ice-cold 10 × hMeDIP buffer (100 mM sodium phosphate pH 7.0, 1.4 M NaCl, 0.5% Triton X-100) and 2 μL 5hmC antibody (Active Motif, 39769) were added to the samples. The samples were rotated at 4°C for 3 hours. 16 μL ProteinG dynabeads (Invitrogen) pre-blocked with 0.5% BSA in PBS were added to the reaction, and rotated at 4°C for 2 hours. The beads were collected on a magnetic rack, and washed three times (with 10 minutes incubations) with 1 × hMeDIP buffer. DNA was eluted from the beads by shaking the samples in 125 μL protease K digestion solution (50 mM Tris-HCl pH 8.0, 10 mM EDTA, 0.5% SDS, 0.2 mg/ml protease K) at 55°C for 30 minutes. Then the DNA fragments were purified using a QIAquick MinElute kit (QIAGEN, 28004). 5hmC levels at promoters of specific genes were further analyzed via qPCR with the designed primers in Table S2. Ten percent of the total genomic DNA from the nuclear extract was used as the input. The fold enrichment was shown after normalizing to the input.

Methylation-specific PCR and bisulfite sequencing

Genomic DNA was extracted using a genomic DNA extraction kit (TIANGEN, 69504) according to the manufacturer's instructions. A total of 1 μg of DNA was used for bisulfite conversion. For methylation-specific PCR, bisulfite-modified DNA was amplified with methylation-specific primers for Dll3 and Notch1, designed by MethPrimer (http://www.urogene.org/methprimer/) and listed in Table S2. Nested PCR was performed using 2 × Taq PCR Mix (TIANGEN, KT201) with following program: initial denaturation at 95°C for 5 minutes, then 36 cycles: 95°C for 30 s, 55°C for 30 s and 72°C for 30 s followed by 72°C for 5 minutes as a final extension. Amplified PCR products were gel-purified with the QIAquick Gel Extraction Kit (QIAGEN). The cDNA was then cloned into the pMD19-T vector (Takara) and transformed in competent *E. coli*. Eight to ten colonies were randomly chosen for sequencing.

Quantification of hydroxymethylated DNA levels

Global DNA hydroxymethylation levels were measured using the MethyFlash Hydroxymethylated DNA Quantification Kit (Epigentek, colorimetric) according to manufacturer's instructions. Signals were detected using the Microplate Reader (BioRad, SpectraMax M5).

QUANTIFICATION AND STATISTICAL ANALYSIS

GraphPad Prism 5.0 (GraphPad Software) was used for the data analysis, and the data are presented as the means ± the standard error of the mean (SEM) for at least three independent experiments. Comparisons among means were performed by one-way analysis of variance (ANOVA) followed by Bonferroni multiple-comparison test for multiple (> 2) groups or two-tailed Student's t test for comparing two means of independent samples. Differences were considered to be significant at $p < 0.05$, $p < 0.01$, and $p < 0.001$. The statistical details for each analysis shown were stated in the respective figure legends.